BRNO UNIVERSITY OF TECHNOLOGY
VYSOKÉ UČENÍ TECHNICKÉ V BRNĚ

FACULTY OF CIVIL ENGINEERING
FAKULTA STAVEBNÍ

INSTITUTE OF STRUCTURAL MECHANICS
ÚSTAV STAVEBNÍ MECHANIKY

SMOOTHED PARTICLE HYDRODYNAMICS IN STRUCTURAL DYNAMICS
SMOOTHED PARTICLE HYDRODYNAMICS VE STRUKTURÁLNÍ DYNAMICE

DOCTORAL THESIS STATEMENTS
TEZE DISERTAČNÍ PRÁCE

AUTHOR — Ing. Martin Hušek
AUTOR PRÁCE

SUPERVISOR — doc. Ing. Jiří Kala, Ph.D.
VEDOUCÍ PRÁCE

BRNO 2021

Keywords

Concrete; Explosion; Impact; Kernel; LS-DYNA; Smoothed Particle Hydrodynamics; Structural Dynamics.

Institute of Structural Mechanics
Faculty of Civil Engineering
Brno University of Technology
Czech Republic

Bibliographic Citation

HUŠEK, Martin. *Smoothed Particle Hydrodynamics in Structural Dynamics*. Brno, 2021. 295 p. Doctoral thesis. Brno University of Technology, Faculty of Civil Engineering, Institute of Structural Mechanics. Supervised by doc. Ing. Jiří Kala, Ph.D.

Table of Contents

1 Introduction

Since the thesis is divided into several parts, a brief introduction with outlines and goals of the thesis is presented first.

1.1 Outline of the Thesis

In **Chapter 1** *Introduction*, the outline of the thesis is discussed. The outline should serve as a detailed table of contents in which a reader can find what is the focus of each chapter. The goals of the thesis are also summarized here. In **Chapter 2** *Smoothed Particle Hydrodynamics*, the Smoothed Particle Hydrodynamics (SPH) method is discussed in detail. First, the early beginnings and development of SPH are reviewed, the mathematical formulation of SPH follows. A detailed examination of kernel functions together with their comparison are part of the chapter. The implementation of SPH in simulations with material strength is also discussed. In **Chapter 3** *From Theory to Application*, the logic of SPH is demonstrated in several tests and benchmarks. The purpose of the chapter is to provide a transition from the mathematical definition to the real application. Some numerical difficulties of SPH are pointed out here. In **Chapter 4** *Coupling SPH and FEM*, the most popular approaches for SPH and the Finite Element Method (FEM) coupling are reviewed. Since it can be problematic to use FEM in certain applications, coupled SPH-FEM models might be the answer. In **Chapter 5** *Quasi-Brittle Materials*, the focus is on quasi-brittle materials in the SPH framework. Discussed is the Continuous Surface Cap Model (CSCM) which is one of the few models that supports strain-rate effects, kinematic hardening, moduli reduction, and strain softening. The performance of the model with SPH on real experiments is evaluated in the chapter. In **Chapter 6** *Reinforced Concrete*, approaches for quasi-brittle materials reinforcement in the SPH framework are described. Since SPH suffers from the so-called tensile instability, it is in fact quite difficult to simulate a reinforcement in concrete. The tensile instability is a numerical error which leads to a false crack development in material. For that reason, the author proposes a new sublayer coupling approach with FEM elements which are not affected by the tensile instability. In **Chapter 7** *Heterogeneity in Numerical Models*, a new approach for material heterogeneity implementation into numerical models is proposed. Due to the Lagrangian nature of SPH, properties of particles might vary over domains and create fields of randomness. However, an uncorrelated random variation results into increased brittleness of the model. For that reason, the author proposes a new approach with which fractal-based noise functions are used to generate a structure of concrete into which the numerical heterogeneity is introduced. In **Chapter 8** *Experiment – High Velocity Impact*, experimental measurements together with numerical simulations are presented. The chapter demonstrates strengths and weaknesses of SPH on a real experiment in which

a high velocity impact (HVI) on concrete specimens was the subject of the study. The newly proposed reinforcement approach, performance of SPH with CSCM, and ability of SPH to predict a dynamic fracture propagation are discussed in the chapter. In **Chapter 9** *Experiment – Explosion*, experimental measurements together with numerical simulations are presented. The focus of the experiment was on responses of concrete slabs subjected to a blast load. The chapter discusses not only the structural parts of the experiment but also the transformation of the explosive into detonation products. A sensitivity study in which the charge orientation was varied is discussed at the end of the chapter. In **Chapter 10** *Conclusion*, the outcomes, findings, and conclusions of the thesis are presented.

1.2 Goals of the Thesis

Since SPH is very well known in fluid simulations, it can be quite challenging demonstrating other possible applications in fields in which mesh-based methods are dominant. As a civil engineer, the author believes that meshfree methods should have a place in structural mechanics and especially in structural dynamics. To change the current state, a clear demonstration of the SPH abilities must be provided. Moreover, an emphasis should be on quasi-brittle materials as it is a fact that concrete and its reinforced variants are preferably used in civil engineering. With respect to that, a list of the goals of the thesis follows.

- Gather information about the SPH history, mathematical background, strengths and weaknesses, recent developments, and state of the art in real applications.
- Prove that SPH is able to pass basic patch tests with a focus on structural mechanics.
- Demonstrate the SPH functionality with plain and reinforced quasi-brittle materials subjected to a static and dynamic load.
- Demonstrate that SPH can be used as an enhancement to standard mesh-based methods.
- Develop a new approach for quasi-brittle materials reinforcement simulated with SPH, free of the tensile instability.
- Develop a new approach for material heterogeneity implementation into SPH models.
- Prove that SPH can represent real experiments in which reinforced concrete specimens are subjected to an impact load.
- Demonstrate the SPH functionality in fluid-structure interaction (FSI) problems.
- Prove that SPH can represent real experiments in which reinforced concrete specimens are subjected to a blast load.

2 Smoothed Particle Hydrodynamics

The first mention of SPH goes to 1977 when Lucy [1] proposed a numerical scheme for obtaining approximate solution of fission problems for optically thick protostars. The SPH as a name however, was not directly used by Lucy but Gingold and Monaghan in [2] in which polytropic stellar models were studied. It is not a coincidence, however, that after SPH was successfully applied in astrophysical problems it was also applied in fluid dynamics (both liquid and gas phases) and high-speed structural dynamics. All three have in common that when particles move and represent either planets, cells of fluid or grains of sand, they can be described by the governing equations of the classical Newtonian hydrodynamics. Hydrodynamics does not mean only fluid simulations but rather fluid-like simulations.

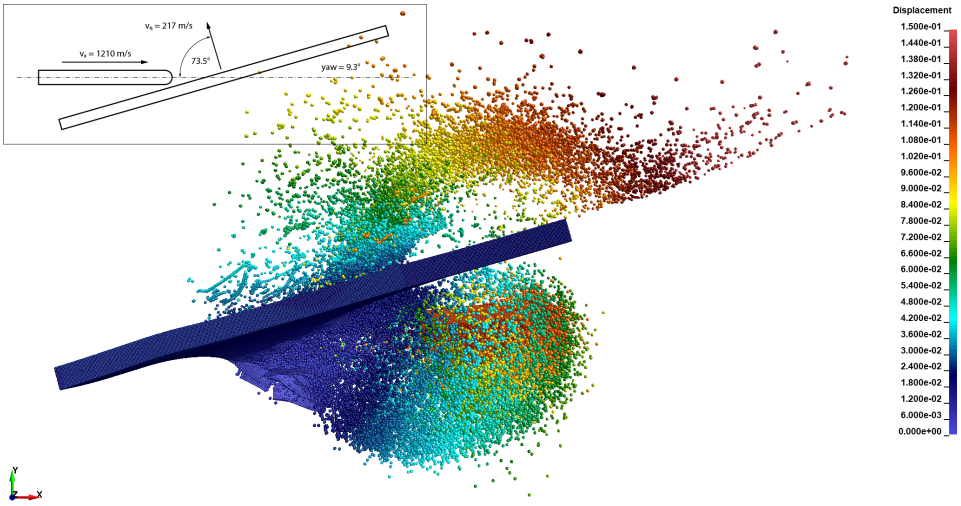

Fig. 2.1. HVI of the depleted uranium alloy long rod projectile into the oblique rolled homogeneous armour plate.

How does it fit into structural dynamics? It depends on how is the 'structural' understood. In the context of the thesis, structural represents *physical strength* of material. Neither concrete nor steel behave like a fluid, however. Yet it really depends on the speed of the event. *When a material with physical strength undergoes deformation very fast, it behaves like a fluid.* A very good demonstration is the impact of the flying uranium alloy long rod projectile on the armour plate as described in the experiment from 1978 [3]. After the impact, both materials behave like fluids; splashing and mixing between each other as shown in Fig. 2.1. The reason for the fluid-like behaviour is simple; the striking velocity was more than 1200 m/s.

2.1 Mathematical Background

As many other numerical methods, SPH was developed to solve problems described by partial differential equations (PDE). The PDEs are not solved directly but after

a domain discretization where the PDEs are defined. For the discretized domain, a field approximation is constructed to obtain a set of ordinary differential equations (ODE). The set of ODEs is than solved with respect to time using some standard integration scheme. SPH uses the concept of shape functions to construct the field approximation. The shape functions, however, are not defined before the solution starts as in the case of FEM but during the solution.

2.1.1 Kernel Approximation

There are several ways to construct shape functions for a field approximation. In case of SPH, the integral representation is used. In literature, the so-called integral interpolant [4], kernel approximation [5], kernel estimation [6], or kernel estimate [7] can be also found. To derivate the kernel approximation, identity where

$$f(\boldsymbol{x}) = \int_{\Omega} f(\boldsymbol{x}')\delta(\boldsymbol{x} - \boldsymbol{x}')\, d\boldsymbol{x}' \tag{2.1.1}$$

can be assumed first. In (2.1.1), f is the function of the position vector $\boldsymbol{x}$ and Ω is the volume of the integral that contains $\boldsymbol{x}$. The $\delta(\boldsymbol{x} - \boldsymbol{x}')$ is the Dirac delta function with a normalization condition. Since the Dirac delta function is used in (2.1.1), the integral representation is exact as long as $f(\boldsymbol{x}')$ is continuous in Ω. The Dirac delta function cannot be used for establishing discrete numerical models since it has only a point support. Therefore, the Dirac delta $\delta(\boldsymbol{x} - \boldsymbol{x}')$ is replaced by a function $W(\boldsymbol{x} - \boldsymbol{x}', h)$ with a support of a finite spatial dimension h, therefore, (2.1.1) became

$$\langle f(\boldsymbol{x}) \rangle = \int_{\Omega} f(\boldsymbol{x}')W(\boldsymbol{x} - \boldsymbol{x}', h)\, d\boldsymbol{x}'. \tag{2.1.2}$$

where W is known as the smoothing function, smoothing kernel function, smoothing kernel, kernel function, or just kernel. In the kernel approximation definition, h is the so-called smoothing length or radius of influence defining the support or influence area of W. Equation (2.1.2) is only an approximation of the integral representation, which is symbolized with the kernel approximation operator, marked by the angle brackets $\langle\ \rangle$. Since the kernel approximation operator is used, there is no approximation but equal sign in (2.1.2).

The kernel might be an arbitrary function, yet it must fulfil certain conditions. The list of conditions is discussed in the thesis in detail. If the kernel conditions are satisfied, the approximation $f(\boldsymbol{x})$ by $\langle f(\boldsymbol{x}) \rangle$ is said to be second order accurate in h [6]. The kernel approximation is not necessarily of second order accuracy if the kernel is not an even function, or if it does not satisfy the normalization condition [5].

2.1.2 Kernel Approximation of Derivatives

The kernel approximation of a function derivatives can be derived by substituting $f(\boldsymbol{x})$ with $\nabla \cdot f(\boldsymbol{x})$ in (2.1.2), which leads to

$$\langle \nabla \cdot f(\boldsymbol{x}) \rangle = -\int_{\Omega} f(\boldsymbol{x}') \cdot \nabla W(\boldsymbol{x} - \boldsymbol{x}', h)\, d\boldsymbol{x}'. \tag{2.1.3}$$

From (2.1.3) perhaps the most important conclusion can be drawn. *The differential operation on a function is transformed into a differential operation on the kernel.* The kernel approximation of the derivative of a field function allows the spatial gradient to be determined from the values of the function and the derivatives of the smoothing function W, rather than from the derivatives of the function itself [8].

2.1.3 Particle Approximation

In SPH, particles can be arbitrary distributed and for the given set of particles the kernel approximation is discretized. The operation is known as particle approximation. This means in practice that (2.1.2) and (2.1.3) are defined in a discrete form.

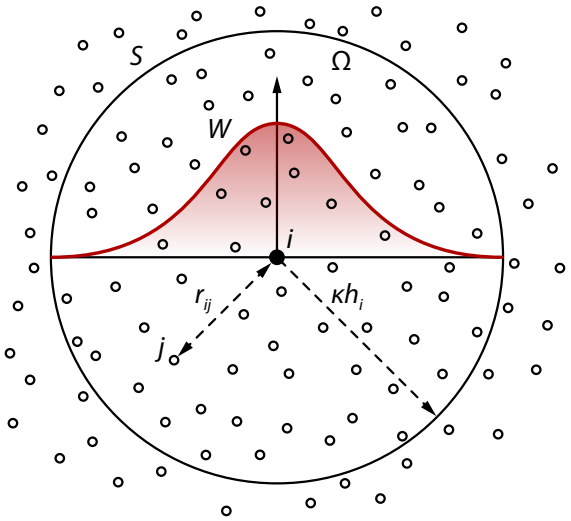

Fig. 2.2. Particle approximation.

To replace the integral in (2.1.2) and (2.1.3), a summation over all the particles within the support domain is introduced. The particles within the support domain of particle i are called neighbouring particles, see Fig. 2.2. Every particle in the problem domain has assigned volume and density. Since volume and density of every particle are given, the mass of particle j can be found as

$$m_j = \Delta V_j \rho_j, \tag{2.1.4}$$

where ΔV_j and ρ_j are the volume and density, respectively. Then discrete forms of (2.1.2) and (2.1.3) for particle i can be expressed as

$$\langle f(\boldsymbol{x}_i)\rangle = \sum_{j=1}^{N} \frac{m_j}{\rho_j} f(\boldsymbol{x}_j) W_{ij}, \tag{2.1.5}$$

and

$$\langle \nabla \cdot f(\boldsymbol{x}_i)\rangle = \sum_{j=1}^{N} \frac{m_j}{\rho_j} f(\boldsymbol{x}_j) \cdot \nabla_i W_{ij}, \tag{2.1.6}$$

where $W_{ij} = W(\boldsymbol{x}_i - \boldsymbol{x}_j, h)$ and N is the number of neighbouring particles, i.e. the particles within the support domain. The particle approximation in (2.1.5) can be understood in the following way. The value of a function at particle i is approximated using the average of those values of the function at all the particles in the support domain (neighbouring particles) of particle i weighted by the kernel [5]. Same applies for derivatives of a function (2.1.6) with one difference, the values of neighbouring particles are weighted by the gradient of the kernel.

2.2 Kernel

Over decades many kernels were formulated. Properties of each kernel differ since they are usually tailored for a very specific application. Yet, they can all be expressed in the form of

$$W(\boldsymbol{x} - \boldsymbol{x}', h) = W(q, h) = \frac{\sigma_{\kappa h}}{h^d} w(q), \tag{2.2.1}$$

where q is the relative distance between two points (particles in practice), d is the number of spatial dimensions, and $\sigma_{\kappa h}$ is the normalization constant. For example, the cubic spline is often considered the standard choice in SPH [9]. It is defined as

$$w(q) = \begin{cases} (2-q)^3 - 4(1-q)^3 & 0 \le q < 1 \\ (2-q)^3 & 1 \le q \le 2 \\ 0 & \text{else,} \end{cases} \tag{2.2.2}$$

with the normalization constants $1/6, 15/(14\pi)$, and $1/(4\pi)$ in 1D, 2D, and 3D, respectively.

2.2.1 Eulerian and Lagrangian Kernel

In essence, there are two types of kernels which are employed in SPH, based on the simulated problem. The difference between them is how they work with neighbouring particles. If neighbouring particles can enter and exit the support domain, the kernel is so-called Eulerian, see Fig. 2.3 (a). In contrast, if neighbouring particles are fixed to the support domain, the kernel is so-called Lagrangian, see Fig. 2.3 (b). In other words, the support domain of the Lagrangian kernel deforms as the particles move in the problem domain. There are other subtypes of the Eulerian and Lagrangian kernels which are discussed in the thesis in detail.

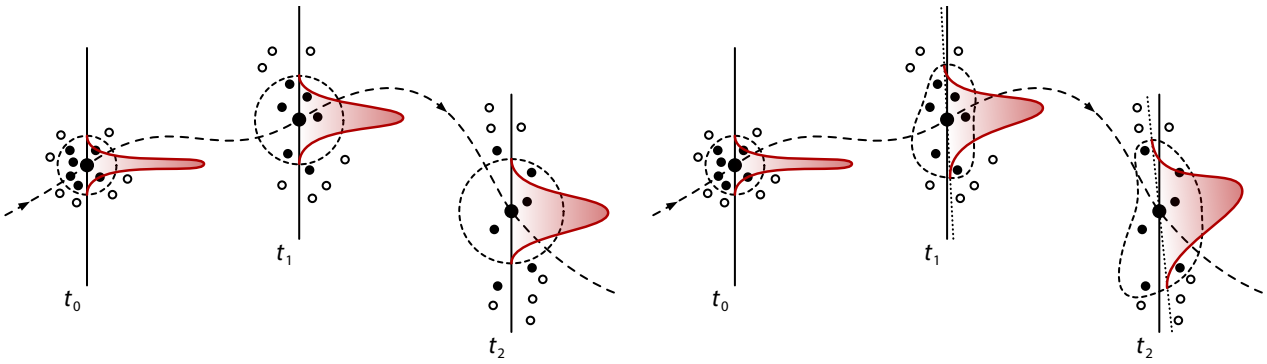

(a) isotropic Eulerian kernel (b) total Lagrangian kernel

Fig. 2.3. Main types of kernels used in SPH.

2.3 Tensile Instability

As any other numerical method, also SPH has shortcomings. To briefly introduce the elephant in the room, the tensile instability is a numerical defect which is closely related to the kernel and stress state. As the name says, the problem was first observed in tensile regions and very often can make an impression of material fracture. However, the fracture is not an outcome of the material model as it is likely to see it even for elastic materials.

In [10], the von Neumann stability analysis [11] was performed to identify conditions which result in the tensile instability. It was proved that the kernel and stress field conditions are the driving parameters. According to [10], the tensile instability depends neither on the artificial viscosity nor on the time integration scheme. The condition or criterion for being stable or unstable was defined in terms of the stress state and the second derivative of the kernel as

$$W''_{\alpha\alpha}\sigma^{+\alpha\alpha} > 0, \tag{2.3.1}$$

where $W''_{\alpha\alpha}$ is the second derivative of the kernel with respect to its argument and $\sigma^{+\alpha\alpha}$ is the total or Cauchy stress tensor. The convention is that the stress component

$\sigma^{+\alpha\alpha}$ is negative in compression and positive in tension. There are no stress or strain thresholds for the onset of the instability [10]. The condition involves only the sign of the product of the total stress times the second derivative of the kernel [10]. A graphical interpretation of (2.3.1) is shown in Fig. 2.4 in which the cubic spline kernel W is plotted together with its first two derivatives W' and W''. There are many ways to alleviate the tensile instability, yet the ultimate solution is to employ the Lagrangian kernel. If the solution with the Lagrangian kernel is extreme and large deformations are being simulated, an acceptable compromise could be using the adaptive Smoothed Particle Hydrodynamics (ASPH) method with the anisotropic Eulerian kernel. Interestingly enough, a lower order kernel with its second derivative everywhere equal to zero is stable in all stress regimes [10].

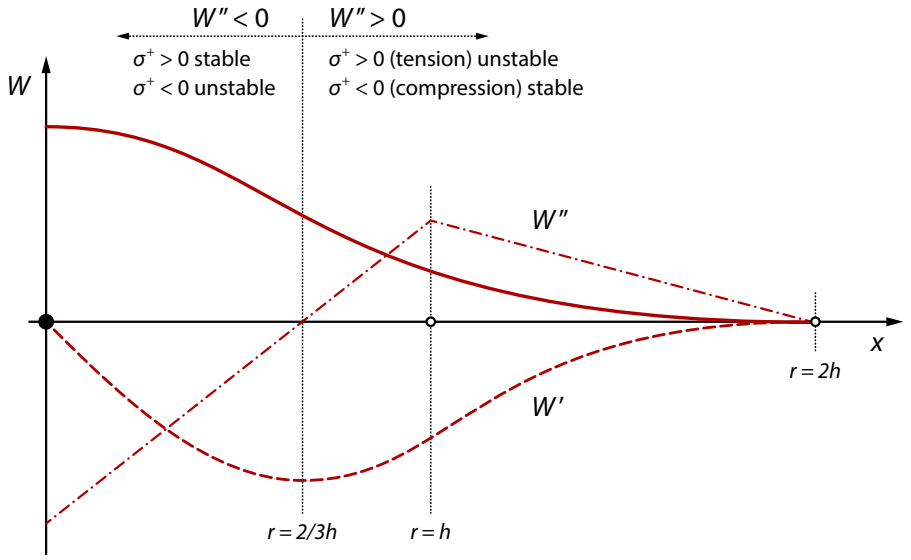

Fig. 2.4. Stable and unstable regions of the cubic spline kernel.

3 From Theory to Application

The chapter serves as a 'bridge' between the theoretical background and numerical modelling. Discussed are the aspects of SPH which might not be obvious from the presented theory.

3.1 Particle Interaction

An important aspect of SPH simulations is the particle interaction. Strictly speaking of the standard SPH, i.e. the formulation with the isotropic Eulerian kernel without corrections, no additional mechanism is needed for the particle interaction between two separate parts. No contact algorithm or coupling is necessary; particles interact between each other when their support domains overlap. However, this built-in mechanism might cause difficulties.

An example in which two flying boxes pass each other can be discussed. A very simple 2D model in which two identical 10 mm × 10 mm boxes with a particle spacing of 0.1 mm fly 300 m/s in opposite directions with a 'distance' between them. The simulations were calculated with the isotropic Eulerian kernel with recommended $h = 1.2\,\Delta x$ and $\kappa = 2$. The Δx and κ are the particle spacing and the support domain scaling constant, respectively. No special treatment was applied to alleviate the tensile instability, no technique to update the smoothing length was used. Furthermore, the material model was linear elastic.

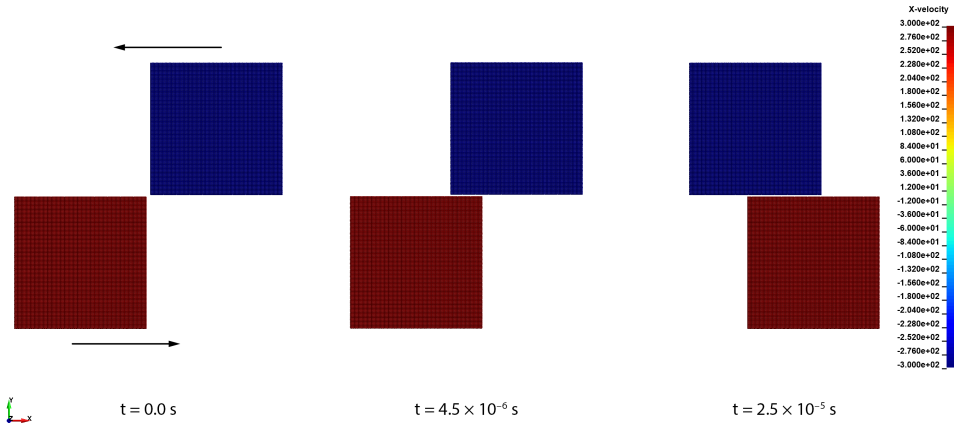

Fig. 3.1. Distance between the boxes 0.24 mm (support size 0.24 mm).

As shown in Fig. 3.1, when the distance is exactly 0.24 mm, no interaction occurs. The reason for this is simple. The specified support domain can influence only the particles within the range of 0.24 mm. Therefore, if the same simulation is calculated with a smaller distance, e.g. with a distance of 0.1 mm, support domains start to overlap and both boxes influence each other as shown in Fig. 3.2. This behaviour is valid from the mathematical perspective and there is no error except the tensile instability. Unfortunately, this is one drawback of how SPH models interact.

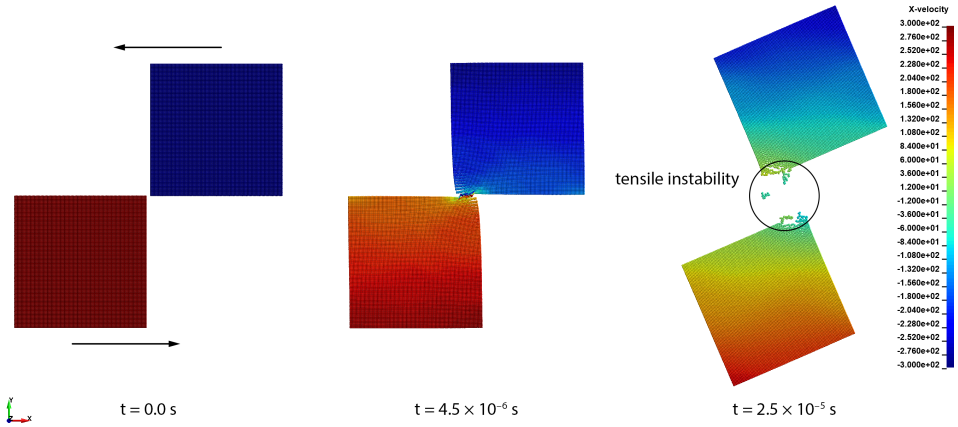

Fig. 3.2. Distance between the boxes 0.1 mm (support size 0.24 mm).

3.2 Tensile Instability Trade-off

The tensile instability can be demonstrated on a simple example in which two rubber rings bounce from each other in high speed. Both rings are identical with the inner radius of 30 mm and the outer radius of 40 mm, only their velocity vector is opposite. The simulations were calculated in 2D, using a particle distribution in a cubic lattice with a particle spacing of 0.5 mm. As shown in [12], the cubic lattice distribution is the most sensitive when it comes to the tensile instability. As in the previous case, the smoothing length $h = 1.2\,\Delta x$ and $\kappa = 2$ were used. Again, the material model was linear elastic.

With regard to the standard SPH, i.e. the formulation with the isotropic Eulerian kernel, even with the renormalization [7], any interaction between two separate parts is handled naturally. This is again due to the adaptive nature of SPH. Yet, in the standard SPH the tensile instability is not treated. Therefore, after the impact, both rings fell apart as can be seen in Fig. 3.3. Why? In the initial state, all the particles have the same velocity, therefore, the stress is constant (zero). After the impact, however, regions of compression (red) and tension (blue) are formed. That can be seen at time 1×10^{-4} s. The instabilities are formed in both regions, yet in tension they are more visible since the particles separate. Although the particles move from each other in the tensile region, the stress does not increase. As a result, the solution is not stable and cracks propagate through the elastic material.

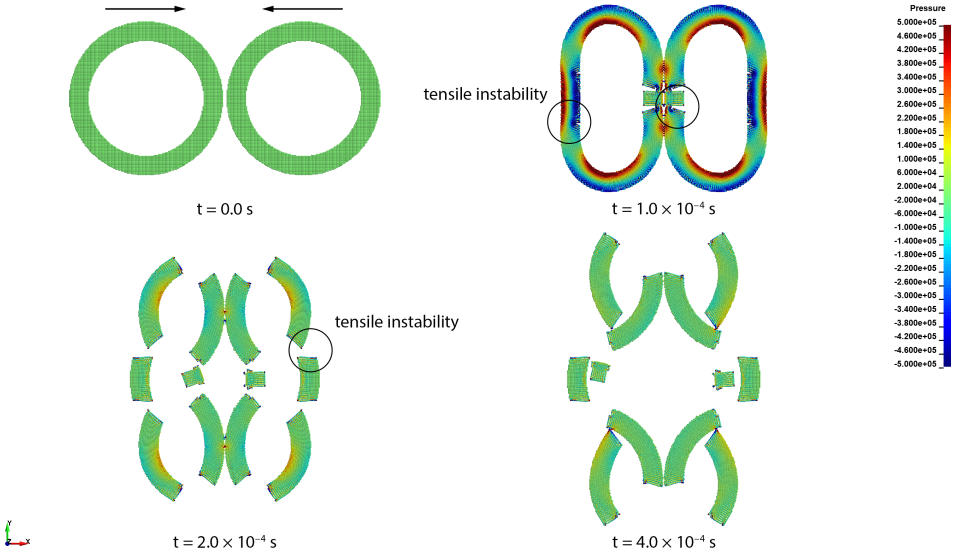

Fig. 3.3. Two elastic rings impact – isotropic Eulerian kernel.

There are many ways to deal with the tensile instability. The easiest solution is to use the total Lagrangian kernel Fig. 2.3 (b). The list of the neighbouring particles is defined during the initialization and never updated. Therefore, the kernel deforms and follows the neighbouring particles as they move. However, SPH is no longer adaptive, there is no update in the neighbouring list. Therefore, the interaction between separate

parts must be treated differently. A possible solution is to introduce a particle contact algorithm, discussed in detail in [13]. Losing the adaptivity of SPH in order to suppress the tensile instability is a bad trade-off.

As shown in Fig. 3.4, using the total Lagrangian kernel indeed solves the tensile instability problem. The regions of compression (red) and tension (blue) are formed again, yet there is no stability issue. Therefore, after the impact at time 1×10^{-4} s, the elastic rings bounce from each other and fly in opposite directions.

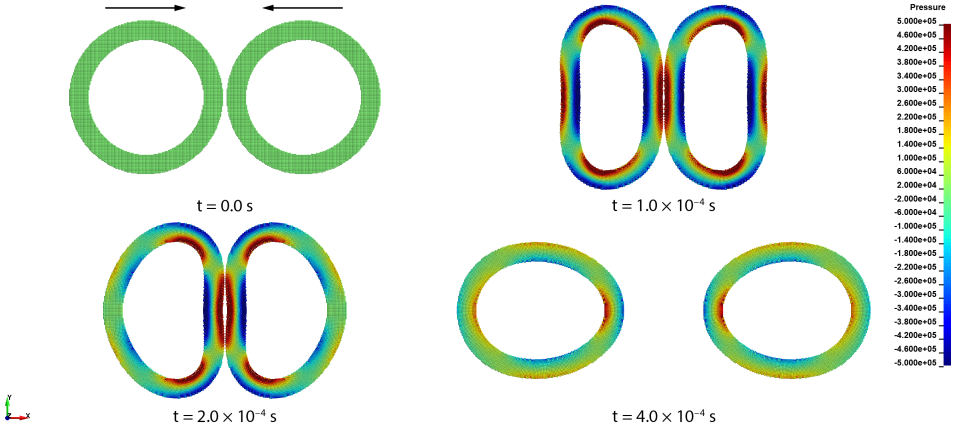

Fig. 3.4. Two elastic rings impact – total Lagrangian kernel.

4 Coupling SPH and FEM

Without a doubt FEM is still the most popular numerical method, not only in the academic circles but in the commercial spheres as well. For that reason the author decided to include FEM as a counterpart mesh-based method to SPH and discuss some useful coupling approaches and techniques. Since both methods are Lagrangian (can be defined as Eulerian, however), the coupling can be done in many ways. In essence, there are three approaches.

- **Penalty-based approach** in which common techniques known from FEM are employed. That would be, e.g. the penalty-based contact algorithm with the nodal penetration detection in which the nodes would be represented by SPH particles.
- **Constraint-based approach** in which one or more degrees of freedom (DOF) are tied. That could be, e.g. when velocities and accelerations of FEM nodes and SPH particles are coupled.
- **Transition layer-based approach** in which the *hybrid* FEM elements are used. The idea is that the hybrid elements contain SPH particles placed inside them, e.g. at locations of the integration (material) points. The motion of FEM elements and SPH particles is again coupled, yet the transition between the hybrid elements and other SPH particles is done with the kernel approximation.

4.1 Comparison of the Coupling Approaches

To see how the coupling approaches perform, an example of a structural deformation can be discussed next. A beam of length 5 m with a rectangular cross-section of $0.25\,\text{m} \times 0.25\,\text{m}$ was fixed on the left-hand side while moved down 0.5 m on the right-hand side. For the comparison purposes, the example was simulated with pure FEM, coupled SPH-FEM with the penalty-based contact, constraint-based contact, and with the transition layer made of the hybrid elements. The pure FEM model is understood as a reference. It is expected that the coupled models result in the same deformation, stress state, and force resistance (force reaction). The coupled models were split into three regions FEM-SPH-FEM. The SPH part of the model was generated from the original FEM part, i.e. each element was replaced by one SPH particle placed at the centre of gravity (CG) of the original element. In case of the transition layer-based approach, the first neighbouring FEM elements were used as the hybrid ones. The material model was linear elastic for all the models.

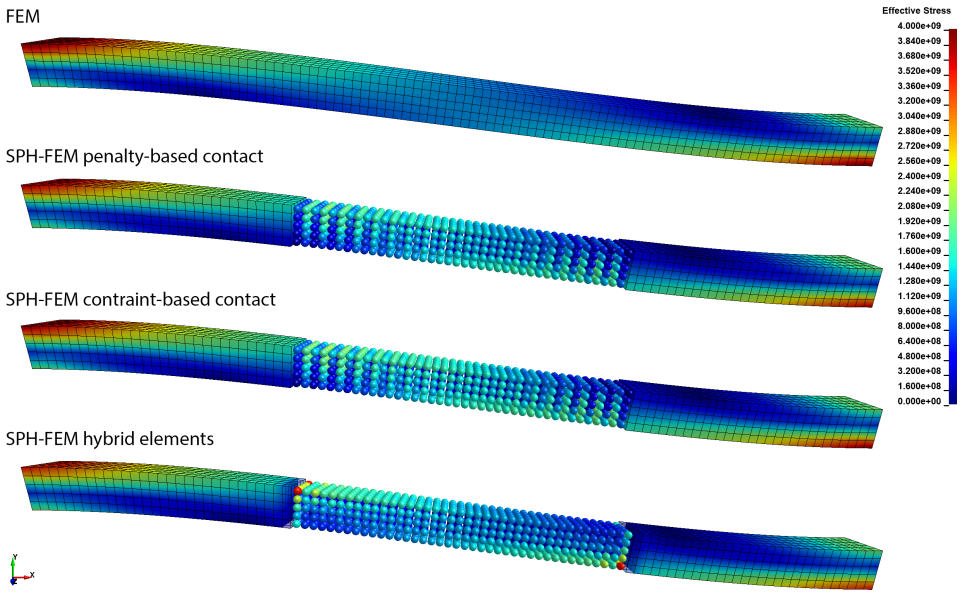

Fig. 4.1. SPH-FEM coupling comparison – effective stress.

Starting with the results in terms of displacements, shapes of all models should be more or less the same. The deformation is smooth, the inflection point is always in the middle as obvious from Fig. 4.1. Yet, when stresses in the form of the von Mises effective stress are compared, the contour distributions are not the same. Taking the pure FEM model as a reference in which contours smoothly transmit along the beam, it is obvious that when the penalty and constraint-based contact is used in the interface, stress oscillations are visible. Oscillations in solutions are nothing new, however. They are well known from the Finite Difference Method (FDM) and FEM where they are referred to as zero-energy modes in general. Similarly, in case of SPH when particles are uniformly distributed, it could happen that the sum of derivatives

is zero since the kernel derivatives are equal in magnitude but opposite in the sign [5]. To completely remove the spurious zero-energy modes, an approach in which additional stress points are used for field functions evaluation was proposed in [14].

The stress oscillations are visible only when the penalty and constraint-based contacts are used for the interface treatment, however. When the stresses are evaluated in the proximity of the interface, it seems that a layer of SPH particles which is in contact suffers with a sudden stress drop. This is of course a singularity in the problem domain and as a consequence the stress field oscillates along the beam till the effect is dispersed. In contrast, in case of the hybrid elements the stress profile is smooth, yet some stress peaks are also visible in the proximity of the interface. In general, the proximity of coupled regions is always problematic since not all conditions of the continuity are enforced.

As discussed in detail in the thesis, from the global perspective the coupled SPH-FEM models return the same responses as the pure FEM model, therefore, all the methods are considered interchangeable and combinable in the discussed extend.

5 Quasi-Brittle Materials

In this chapter, quasi-brittle materials are discussed in terms of the SPH framework. Since the majority of constructions in civil engineering are made of concrete or reinforced variants of concrete, it is natural that the performance of SPH with quasi-brittle materials should be subjected to a thorough investigation. Since it is not the subject of the thesis to benchmark all the available material models, only a representative model is chosen and discussed in detail. Given the variability of load types in structural dynamics, CSCM as the most versatile material model was chosen.

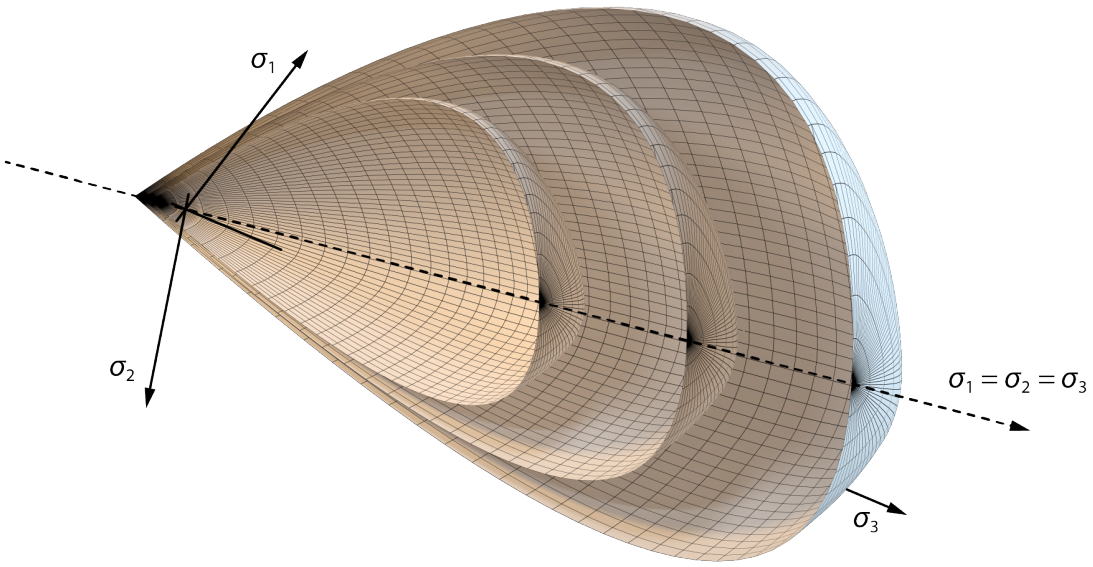

Fig. 5.1. Illustration of a cut through the CSCM yield surface for three different strength classes in principal stress space.

5.1 CSCM Material Model

CSCM is a three-invariant-based material model, specifically designed for use in roadside safety simulations. Since roadside safety is a part of structural dynamics, the author was always able to make of use of it in SPH simulations. The CSCM yield surface is defined with respect to three stress invariants – the first invariant of the stress tensor I_1, the second invariant of the deviatoric stress tensor J_2, and the third invariant of the deviatoric stress tensor J_3. The yield surface f is defined as

$$f(I_1, J_2, J_3, \kappa) = J_2 - \mathcal{R}^2 F_f^2 F_c, \tag{5.1.1}$$

where F_f is the shear failure surface, F_c is the hardening cap, $\mathcal{R}$ is the Rubin three-invariant reduction factor [15], and κ is the hardening parameter that controls motion of the cap. An illustration of the CSCM yield surface in principal stress space for three different strength classes is shown in Fig. 5.1. For different strength classes the yield surface expands or contracts. The expansion and contraction is more pronounced in compression.

5.2 Experiment – L-Shaped Structural Members

To better understand how SPH behaves with quasi-brittle materials, experimental and numerical investigations of the so-called L-shaped structural member or just L-specimen are briefly discussed. The experiment itself is quite simple, only the L-specimen made of plain concrete is needed. The L-specimen is fixed on one side and subjected to imposed loading on the other, therefore, the inner corner is ‘opening’ in time. The focus of the study in the thesis is limited to the highest loading rate of 2400 mm/s which was analysed in [16].

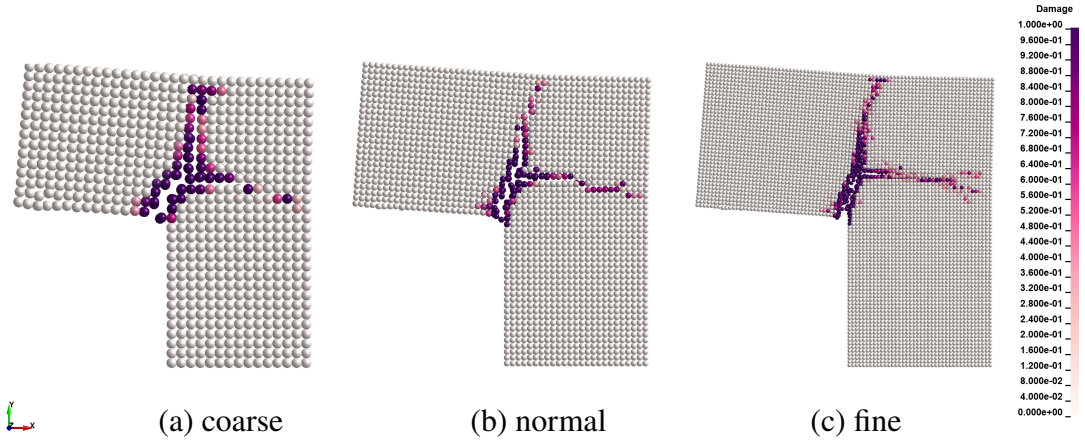

(a) coarse (b) normal (c) fine

Fig. 5.2. Crack patterns comparison for different discretization densities; displacement rate 2400 mm/s.

5.2.1 Influence of the Particle Discretization Density

The first step in the SPH evaluation with CSCM shows the influence of the particle discretization density. Pure SPH models were used with three discretization densities to simulate the experiment. Taking into account the thickness of the L-specimen of 50 mm, the particle spacing of 16.67 mm, 10 mm, and 6.25 mm were tested. That would be the definition of the coarse, normal, and fine model.

As shown in Fig. 5.2, all three models give the same crack pattern which means that the discretization density have just a minor impact on the results and the fracture energy normalization implemented in CSCM works as expected. In numerical methods, the discretization density plays significant role in both space and time. With the results shown in Fig. 5.2 it was proved that SPH is stable when it comes to the qualitative comparison of discretization levels and that the brittle behaviour can be successfully simulated with it. Other evaluations are discussed in the thesis.

5.3 Experiment – Concrete Spalling

As discussed in **Chapter 4** *Coupling SPH and FEM*, it is not always necessary to use pure SPH models, especially when an existing model is already built and SPH is used just as an enhancement. For example, a FEM model can be a starting point for an HVI debris simulation. However, it is quite difficult to simulate spalling and scabbing of concrete with FEM. For SPH, on the other hand, it is not a problem at all. But how to transform FEM into SPH during the simulation?

5.3.1 Element Erosion

The idea of the SPH and FEM coupling in HVI debris simulations is quite straightforward. At the beginning, there is only a FEM model with assigned brittle material, e.g. with CSCM. After the model is subjected to the impact and the load-carrying capacity of the FEM elements is reached, the elements have no stiffness, therefore, a little purpose to remain active. In other words, the elements can be eroded since they represent debris. Mass cannot just disappear, however. A possible solution is to transform the failed elements into SPH instead. The mass and energy are preserved and the simulation can advance in time but as coupled SPH-FEM.

To better understand the concept, an example is shown in Fig. 5.3 in which three concrete blocks impact a rigid surface. It is clear from the results that a simple element erosion leads to an error in the simulation, since the mass and energy just simply dissipate, disappear. However, when the eroded mass is transformed into SPH, the results again correspond to the original FEM solution without the element erosion. This rather simple example shows a complex technique with a potential in structural dynamic applications. The author used the described technique in simulations of an

HVI experiment to further study the behaviour of coupled SPH-FEM models. Due to the limit size of the thesis statements, only results of the simulated experiment [17] are discussed.

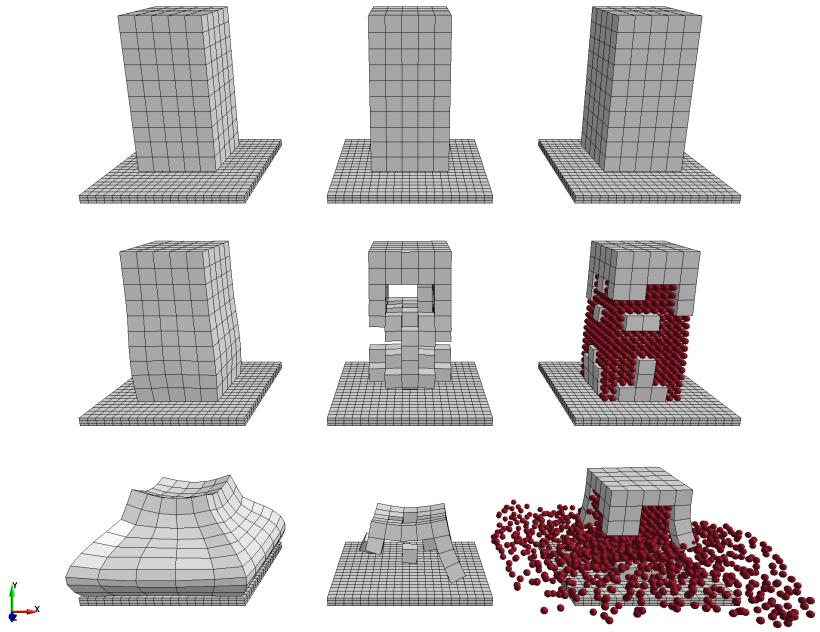

(a) no erosion (b) erosion (c) erosion into SPH

Fig. 5.3. Three models comparison in a simple HVI simulation.

In 2001 Buchar et al. [17] performed an experiment in which concrete blocks were impacted by steel projectiles accelerated to different velocities. Three numerical models with the same logic as shown in Fig. 5.3 were used to simulate the experiment. The first model was a standard FEM model without the element erosion. The second and third model allowed the element erosion when the CSCM damage value of 1 was reached. The third model, however, transformed the eroded mass into SPH particles, therefore, the mass and energy were preserved.

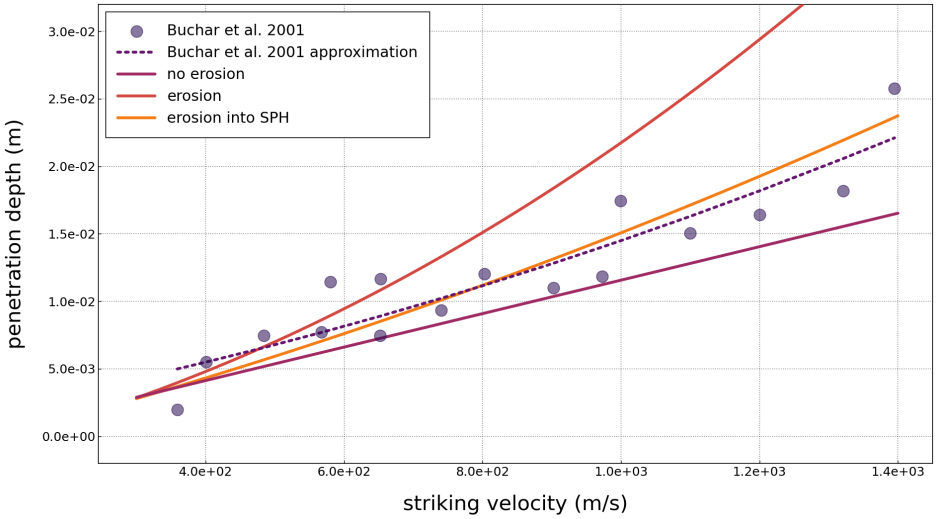

Fig. 5.4. Penetration depths over the range of striking velocities.

From the comparison of penetration depths in Fig. 5.4 it is clear that the experimental measurements were reproduced quite well by the model without the erosion and the model with the erosion and transformation of the eroded mass into SPH. Responses of all three models are almost identical for striking velocities below 400 m/s. For moderate and high striking velocities, however, the simple model with the element erosion is inapplicable.

6 Reinforced Concrete

In terms of plain concrete, SPH can be very useful and offer much more than standard mesh-based methods. Reinforced concrete, however, might be a problem. Again, the tensile instability is to blame. Sometimes might be useful however to borrow pieces from other methods and use them as an enhancement in SPH. In this chapter, the concept of a reinforced concrete modelling with SPH is discussed.

6.1 Sublayer Coupling with FEM

As shown in the thesis in detail, due to the tensile instability it might be difficult to simulate a reinforcement in concrete since numerical cracks develop prior reaching the yield strength in the reinforcement. Of course, this is a problem of the Eulerian kernels only. However, using the total Lagrangian kernel might not be optimal as well, since models with Lagrangian kernels show a rather stiffer behaviour.

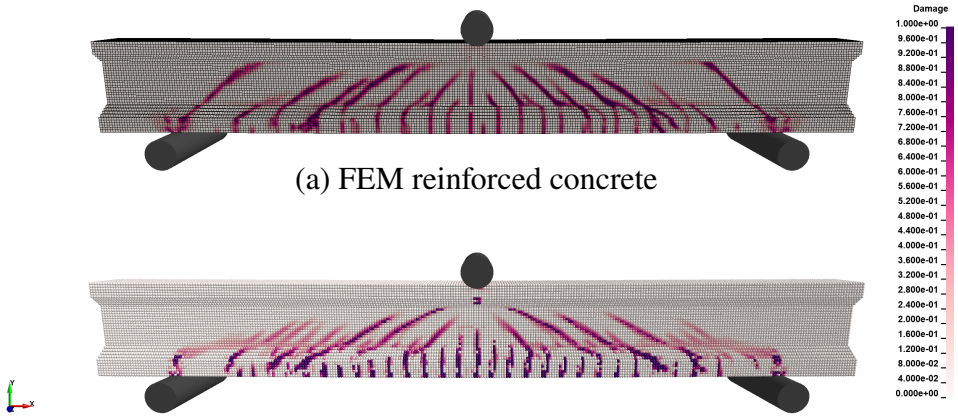

(a) FEM reinforced concrete

(b) SPH-FEM reinforced concrete

Fig. 6.1. Damage comparison of the reinforced I-girder FEM and coupled SPH-FEM model.

To bypass the problem of the tensile instability, the author proposes the following approach as *sublayer coupling* which uses FEM beam elements as an enhancement in otherwise pure SPH models. The idea is based on the oldest coupling approach in which nodes of the concrete and reinforcement are simply shared. However, since the coupling is done between two different yet Lagrangian methods, the logic must be adapted. When two separate FEM parts are being coupled with shared nodes, the

nodes of both parts must have identical locations. In SPH it is not necessary due to the adaptive nature of SPH. In other words, the particles representing the concrete can be arbitrary distributed and the beam elements can be freely placed within the particles. To create a connection between them, every FEM node must become also an SPH particle. Then the connection is done naturally since support domains of the concrete and steel particles overlap. The artificially generated SPH particles represent the *sublayer* for coupling. There are important aspects which must be considered, however. As discussed in the thesis in detail, the total mass of the reinforcement must be represented while masses of SPH particles and FEM nodes must not be zero. The ratio of the masses leads to different coupling forces, stiffness distribution, time step in the integration scheme, and overall response. The author has found that the ratio of equal mass distribution works in the most cases.

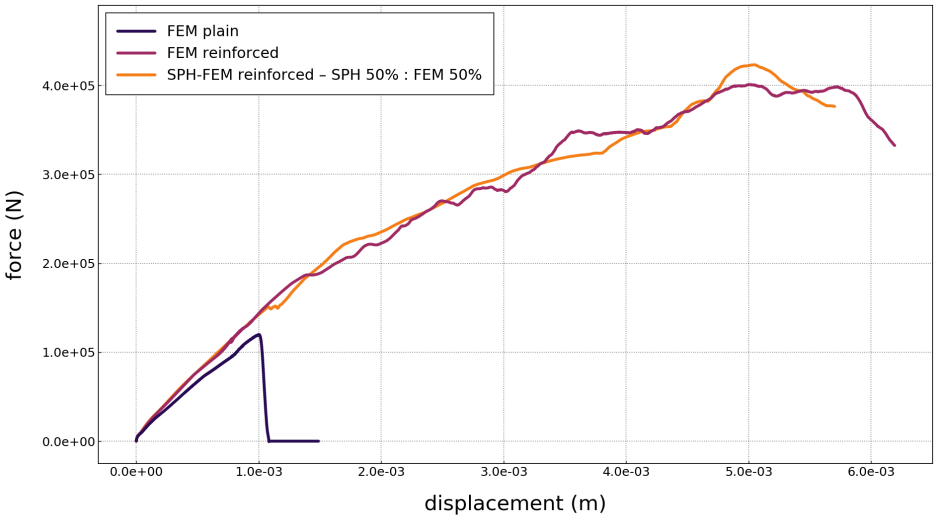

Fig. 6.2. Force-displacement diagrams comparison of selected models.

A simple demonstration of the coupling approach in a three-point flexural test of a reinforced I-girder with steel can be discussed. Having a pure FEM model as a reference, an SPH model with the sublayer can be simple created using the FEM elements. When the coupled model is generated, it consists of three parts – the SPH concrete, SPH reinforcement sublayer, and FEM reinforcement. A comparison of damage states after the ultimate load-carrying capacity was reached is shown in Fig. 6.1. Clearly, both models show a similar behaviour. The coupled model used the equal mass distribution. Responses in terms of a force reaction are shown in Fig. 6.2. Again, both models show a similar response, free of the tensile instability.

7 Heterogeneity in Numerical Models

In real life, in experiments, nothing is entirely perfect. Concrete specimens are not always straight, sometimes even pre-cracked, boundary conditions are never

symmetric even when intended. This is the reason why experimental measurements exhibit differences. With every specimen, with every measurement, there is a deviation. Crack patterns are not always the same, peak forces very often vary, initial stiffness might be influenced by the testing device itself. However, in simulations, everything can be 'perfect'. There is no deviation in geometry, material parameters are as defined, and when the model is symmetric, well, it is symmetric. But what if some variations should be in the model, what if the simulation results should exhibit a certain degree of randomness? In this chapter, the so-called *numerical heterogeneity* is discussed.

7.1 Randomness – Much Ado About Nothing?

When it comes to randomness, there are many ways to implement it into numerical models. For example, material strength can vary in the problem domain which results in a random failure. The question is, however, how to pass the information with the modified strength to SPH particles. As discussed in the thesis in detail, since particle masses and densities are directly used in the particle approximation, therefore, in the kernel approximation operations, they can vary in the problem domain. This would be considered the simplest numerical heterogeneity implementation.

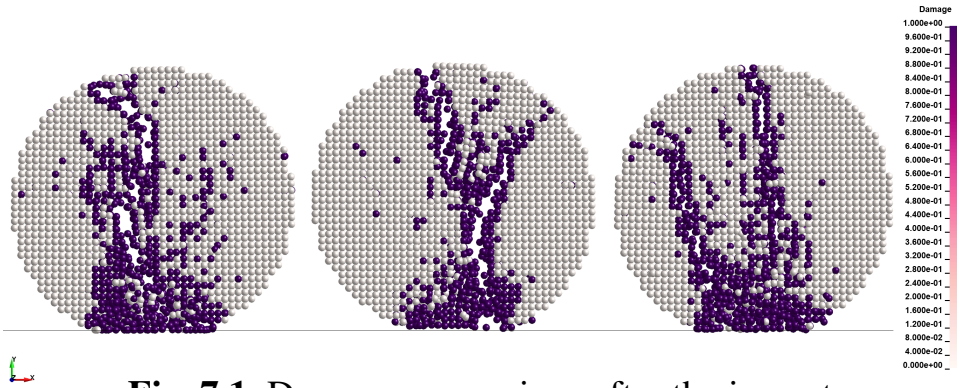

Fig. 7.1. Damage comparison after the impact.

As shown in Fig. 7.1 in which three concrete disks impact a rigid surface, the behaviour of each disk is indeed unique, random. The reason for this is that each disk was generated with a random mass distribution. However, the mass oscillations resulted into increased brittleness. The presented approach of the numerical heterogeneity implementation can be used in simulations in which constitutive equations are not important. For a general use, however, the approach for the numerical heterogeneity implementation must be improved.

7.2 The Algorithm

The concept of the parameters oscillations can be used with SPH, but the regions where the parameters differ must be generated differently, not randomly. For the reasons mentioned, the author proposes the *algorithm for concrete structure generation* with

which a spatial geometry of a concrete is generated and further used with the concept of the numerical heterogeneity. The generated geometry is based on the mesolevel of concrete, i.e. generated are regions of aggregate, mortar-matrix, and the interfacial transition zone (ITZ). Furthermore, the generated structure can be based on a real photo of a concrete. When an input photo is used with the algorithm, a spatial concrete structure from the photo is recreated. For example, as shown in Fig. 7.2, based on an input photo of a concrete, a spatial geometry of the concrete was recreated. It is quite extraordinary since only a 2D photo was used as the input.

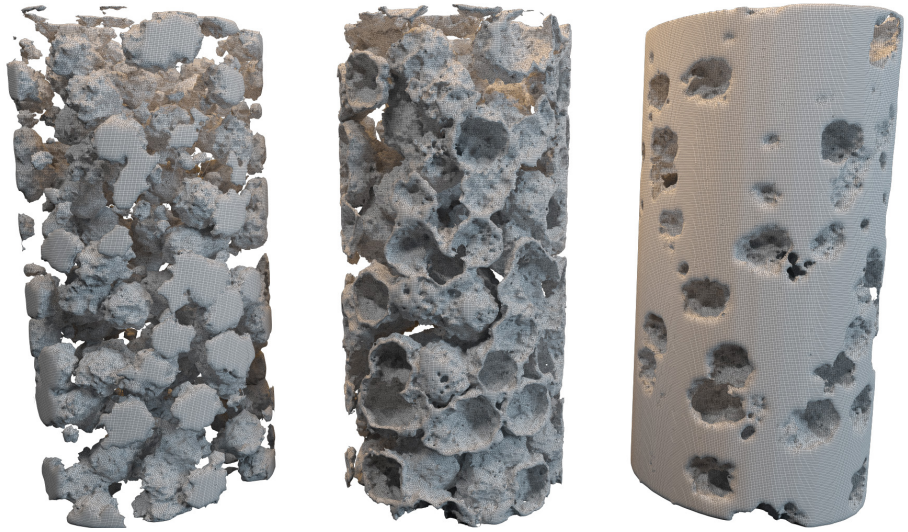

(a) aggregate (b) ITZ (c) mortar-matrix

Fig. 7.2. Generated structure of concrete with sharp aggregate.

With the algorithm for concrete structure generation, 'random' fields can be generated in few seconds. Within these fields, SPH particles can have different properties.

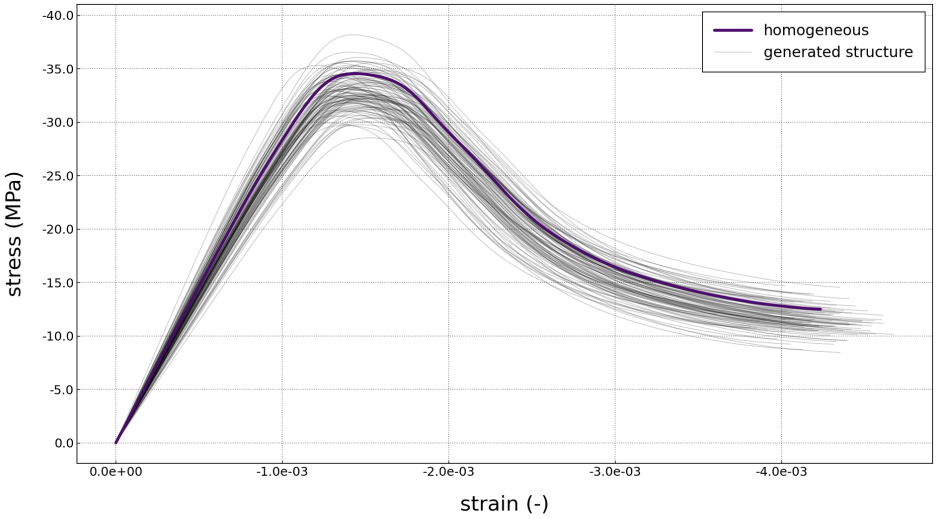

Fig. 7.3. Comparison of uniaxial compressive strengths of the homogenous model and those with generated structure.

If the properties of all particles are identical in all domains, the model is again homogenized (macrolevel). If the properties differ, the model is with the numerical heterogeneity (mesolevel). The properties do not have to vary in all domains, however. It could be that CSCM is used as a base material, yet in the ITZ domain the unconfined or uniaxial compressive strength (UCS) or density varies. The approach of the strength variation within the ITZ domain was used in UCS simulations on cylindrical concrete specimens. As shown in Fig. 7.3 in which stress-strain diagrams are collected for the initial homogenous model and generated 100 samples, randomness in behaviour was achieved yet in meaningful sense.

8 Experiment – High Velocity Impact

In this chapter, a numerical simulation of an HVI experiment which was performed by the author and his colleagues is discussed. The chapter serves as a proof that SPH is indeed a proper tool when it comes to structural dynamic simulations in which concrete is employed.

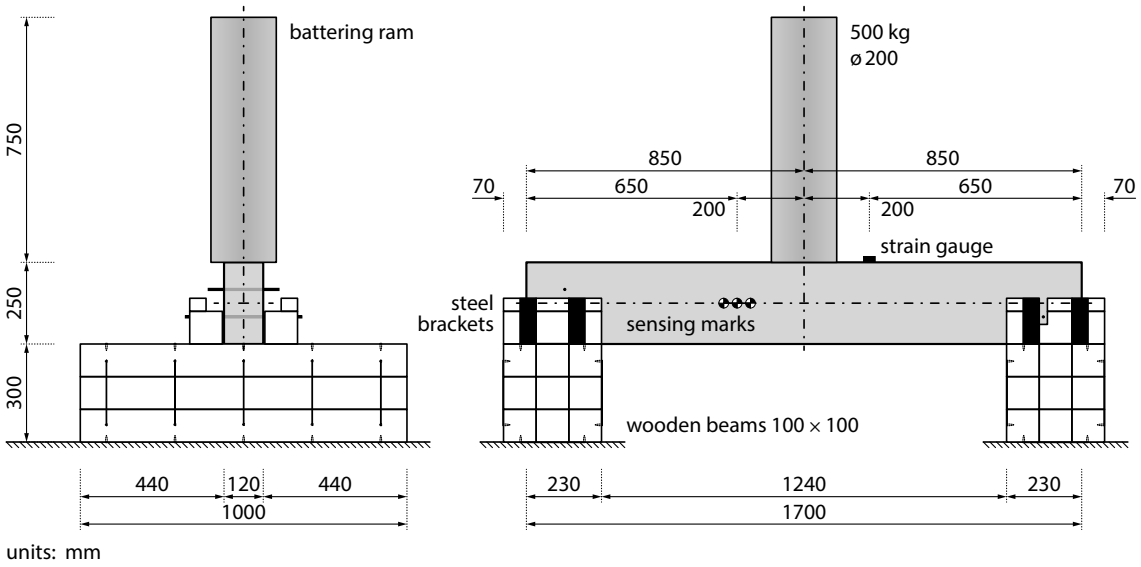

Fig. 8.1. Schema of the HVI experiment.

8.1 Experiment Description

The experiment can be described as an impact test in which the focus is on the impacted specimen rather than on the impactor. In this particular case, the specimen was a reinforced concrete beam and the impactor was a steel battering ram. A schema of the experiment can be seen in Fig. 8.1. Since the battering ram was 500 kg and the drop height was 0.95 m, concrete class C30/37 [18] and steel class B500B [18] were used. Three responses were studied in detail – longitudinal strain at the top surface of the beam during the impact, vertical displacement in the middle of the height of the beam during the impact, and damage of the beam after the impact.

8.2 Measurements

Seven specimens were tested in total, all with the same drop height of 0.95 m. The first two measurements were used for in-situ calibration purposes, therefore, they are not included in the result overview and were not considered for the material calibration. Each specimen had its own identification code starting with '7IX' and a number (3 to 7).

Fig. 8.2. Damaged specimen 7IX-4 after the impact.

Since all the tested specimens ended in the same damage state as shown in Fig. 8.2, i.e. the failure mode, crack pattern, and size of the damaged region, therefore, specimen 7IX-4 can be understood as a reference for the numerical simulations.

8.3 Numerical Model

The numerical model was not a pure SPH model but a coupled with FEM. The main reason for using the coupled model was computational requirements. It would be impractical to use SPH in regions of a lower importance, since SPH can be quite expensive in terms of computational requirements. Therefore, FEM was used mainly for the supports. The reinforcement was modelled with the proposed coupled SPH-FEM sublayer approach. The SPH part of the model (the concrete) was generated into a cubic lattice with a particle spacing $\Delta x = 6 \pm 0.05$ mm in all three directions. This resulted in more than 255,000 SPH particles in total, including those in the reinforcement sublayer for the FEM coupling. Tested were two model variants with and without the CSCM strain-rate effects.

8.4 Results

Since the goal of the thesis is to provide a proof of the SPH functionality when used in structural dynamics, the calibration of the material parameters is not discussed

here but is being published separately to the thesis. The calibrated model is however discussed in terms of the SPH performance. Note that negative displacements stand for a movement downwards and negative strains mean longitudinal compression.

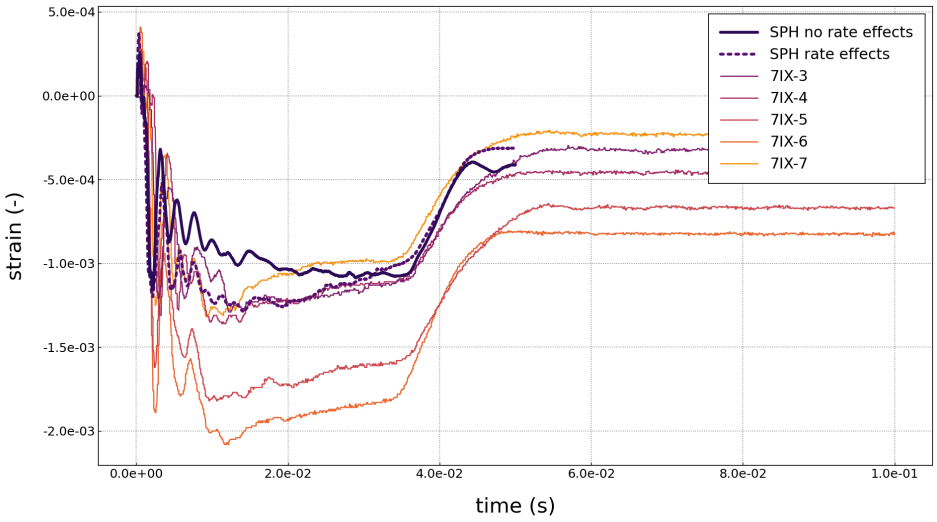

Fig. 8.3. Strain at the top surface of the beam over time.

As shown in Fig. 8.3 in which strains over time are compared, both SPH models reproduce the measurements quite well. The model with the strain-rate effects predicts the strain responses slightly better, as it seems that all the gradients fit quite nicely. Both models represent rather a lower bound of the measurements, not the mean, however.

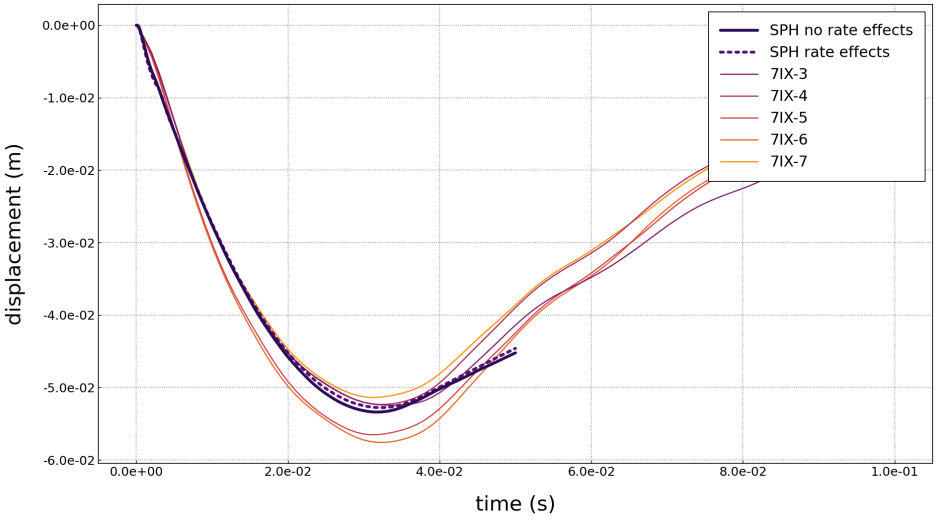

Fig. 8.4. Displacement at mid-span of the beam over time.

Displacements in Fig. 8.4 are also quite nicely represented by both models. Yet, only down to the peak, the unloading branches show some differences. The initial loading branches (movement downwards) show almost identical rate (stiffness) and peak

values as in the experiment. As it was the case for the strains, also the displacements represent rather a lower bound of the measurements.

Since there are only minor differences in damage states of both models, only the model without the rate effects is discussed next. The damage state of the concrete at the end of the simulation is shown in Fig. 8.5. When compared to the photo in Fig. 8.2, it is without a doubt that the model represents the crack pattern quite well. The model shows concrete crushing in the contact region with the battering ram, and a flexural and shear cracking as in the experiment. From a closer look it might seem that the model is burdened with the tensile instability at the bottom part. However, it is not the case. The opening is truly material opening.

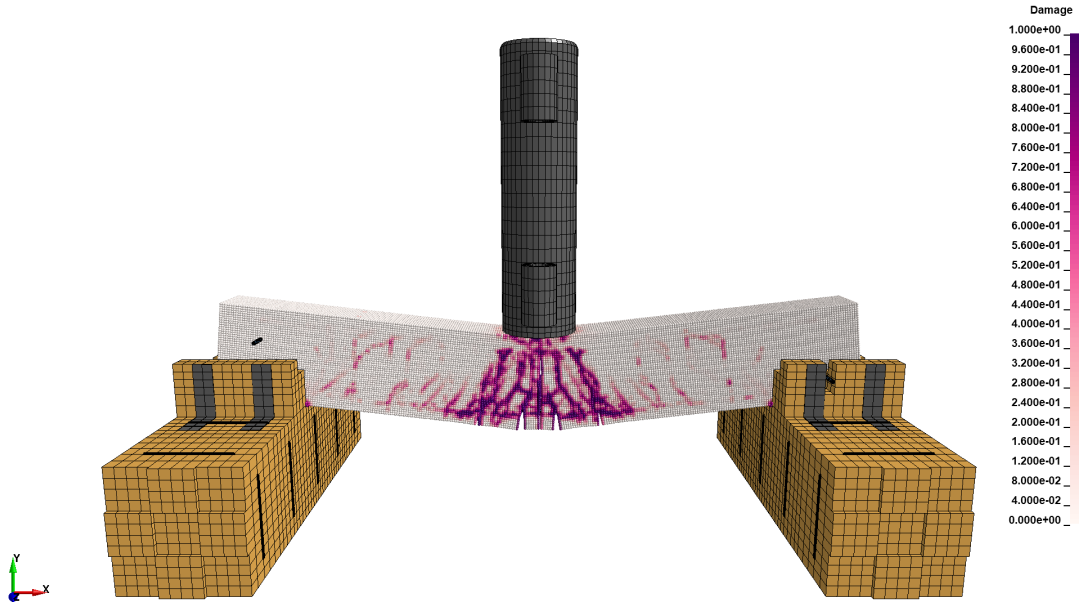

Fig. 8.5. Damage of the model without the CSCM strain-rate effects.

Strictly speaking of the SPH part of the model, no stability issues or other numerical problems were observed. Both models were free of the tensile instability. The fact that the coupled SPH model was able to capture all the responses of the experiment is not only a proof that SPH is fully functional and can be used in civil engineering applications, but also that the proposed *sublayer coupling* approach works.

9 Experiment – Explosion

As in the previous chapter, a coupled SPH model with FEM is used to simulate what was observed in an explosion experiment. This time, however, SPH simulates both structural parts and fluids. The experiment was performed by the author's colleagues, who also provided the measurements, for which the author is grateful. The goal of the experiment was to analyse the behaviour of a reinforced concrete slab exposed to a close-in explosion with a stand-off distance only few centimetres. Although the simulation results show a good agreement with the experimental measurements,

some differences were found. To understand the differences better, a sensitivity study of uncertain parameters was performed.

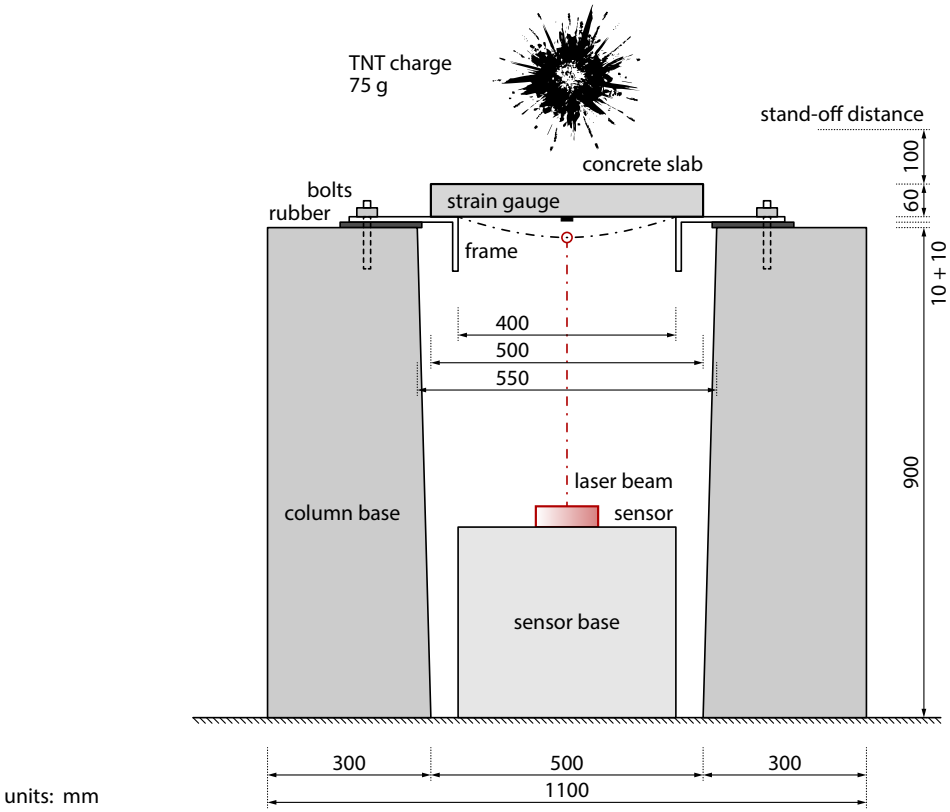

Fig. 9.1. Schema of the explosion experiment.

9.1 Experiment Description

The experiment was designed to study a close-in explosion, i.e. when a charge (an explosive) is placed and detonated relatively close to the examined specimen. The specimen was a reinforced concrete slab of standard concrete class C30/37 [18] and a steel reinforcement of class B500B [18]. A schema of the experiment is shown in Fig. 9.1. The explosive was a standard military 75 g Trinitrotoluene (TNT) charge of a cylindrical shape with a diameter of 30 mm and height of 70 mm. The charge was placed above the concrete slab with a stand-off distance of 100 mm. The orientation of the charge was such that the axial axis of the cylinder was perpendicular to the concrete slab. Two responses of the concrete slab were measured over time – displacement and strain at its bottom surface.

9.2 Measurements

Six specimens were tested in total, yet, one of the specimens was damaged in a rather non-standard way, therefore, it is not shown in the result overview and was not considered for the material calibration. Each specimen had its own identification code starting with ‘4X’ and a number (1 to 6, number 4 skipped). In addition to the

measurements of strains and displacements, the focus was also on the damage state. For instance, specimen 4X-5 after the explosion is shown in Fig. 9.2. Based on the photo documentation it can be said that the top surface of the specimen shows little to no damage but rather a blackened pattern caused by the imperfect combustion of the charge. However, the true damage is found at the bottom surface. Several cracks propagate in parallel and diagonal directions all the way through the specimen.

(a) top

(b) bottom

Fig. 9.2. Damaged specimen 4X-5 after the explosion.

Slow motion cameras were employed to provide yet another view into the experiment. In Fig. 9.3, time-lapse of the explosion is shown. The main learning from the time-lapse is the shape of the detonation products and direction of the formed 'spear' in Fig. 9.3 (b) which is related to the shape of the charge.

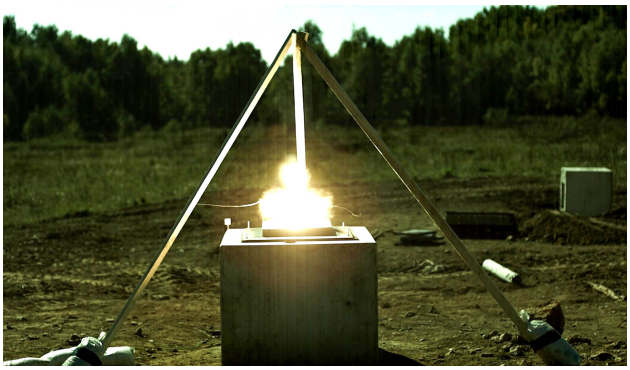

(a) 1.0×10^{-4} s

(b) 1.0×10^{-3} s

Fig. 9.3. Time-lapse of the explosion.

9.3 Numerical Model

The numerical model was again coupled with FEM, yet the load itself (the explosion) was simulated with pure SPH. For the same reasons as in the previous experiment, the support system was modelled with FEM. The concrete portion of the reinforced

slab was modelled with SPH and the reinforcement with the proposed coupled SPH-FEM sublayer approach. The SPH part of the reinforced slab (the concrete) was generated into a cubic lattice with a particle spacing $\Delta x = 5$ mm in all three directions. This resulted in more than 135,000 SPH particles in total, including those in the reinforcement sublayer for the FEM coupling. Tested were two model variants with and without the CSCM strain-rate effects.

9.4 Results

As shown in Fig. 9.4 in which strain diagrams are compared, the overall trend was captured quite well by both models with and without the rate effects. The peak value in tension of both models is comparable with the peak measured in the experiment. Both models show a rather brittle behaviour, however. Unfortunately, only one measurement was obtained from the experiment.

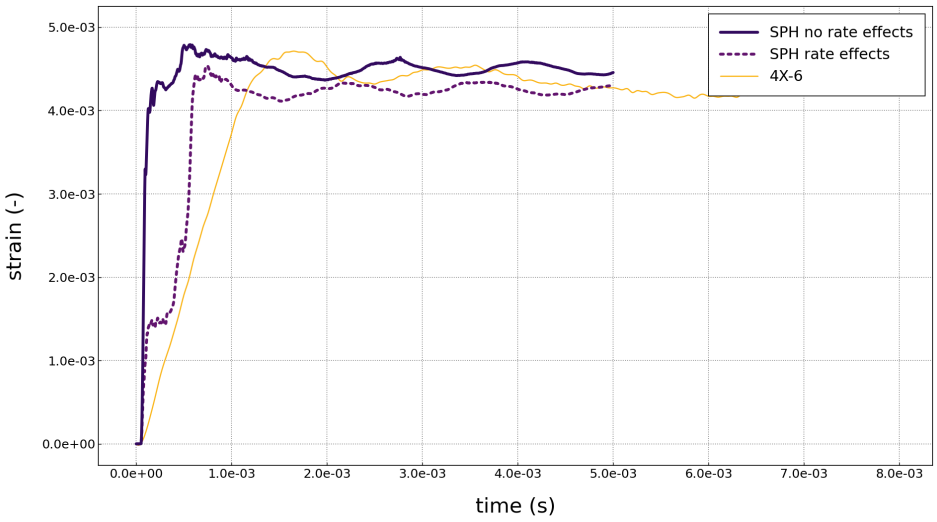

Fig. 9.4. Strain at the bottom surface of the slab over time.

The comparison of displacements in Fig. 9.5 shows again a good agreement between both simulations and the experimental measurements. The gradient of the initial motion downwards is quite well captured for four out of the five specimens. The reason for this is that the initial part shows only the displacement or rather the deflection of the concrete slab itself, yet not the deformation of the support system.

Although the result comparisons in Fig. 9.4 and Fig. 9.5 show that the model with the rate effects might reproduce the measurements better, it is not the case in terms of the damage. The model with the rate effects yields formation of a region where micro-cracks dominate. This is in contrast to the experiment in which only main cracks were observed. For that reason, only the model without the rate effects is shown in Fig. 9.6.

As previously shown in Fig. 9.2, the top surface of the slab was relatively undamaged. Almost the same picture can be seen in Fig. 9.6 (a) with perhaps an initialization of a cracking in the middle of the sides. The bottom surface reveals far more interesting results. As can be seen in Fig. 9.6 (b), the crack pattern shows more individual cracks oriented in the diagonal direction rather than in the direction perpendicular/parallel to the sides of the slab. This is perhaps different to the experiment, in which perpendicular/parallel cracks were observed as well.

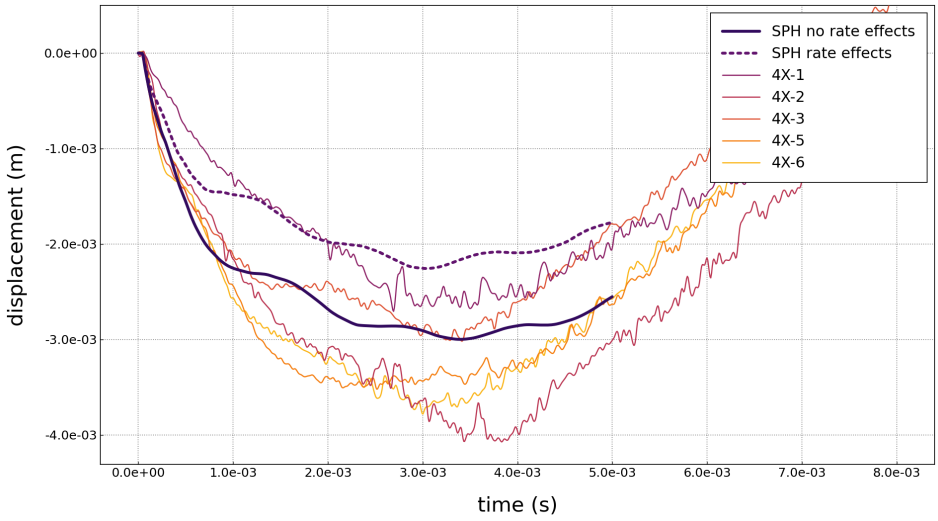

Fig. 9.5. Displacement at mid-span of the slab over time.

The SPH charge performed well, there were no stability issues in FSI. When the SPH particle distribution in Fig. 9.7 is compared to the detonation products in Fig. 9.3, it is quite impressive how are the profiles similar. It is just another indicator that SPH can simulate FSI quite well.

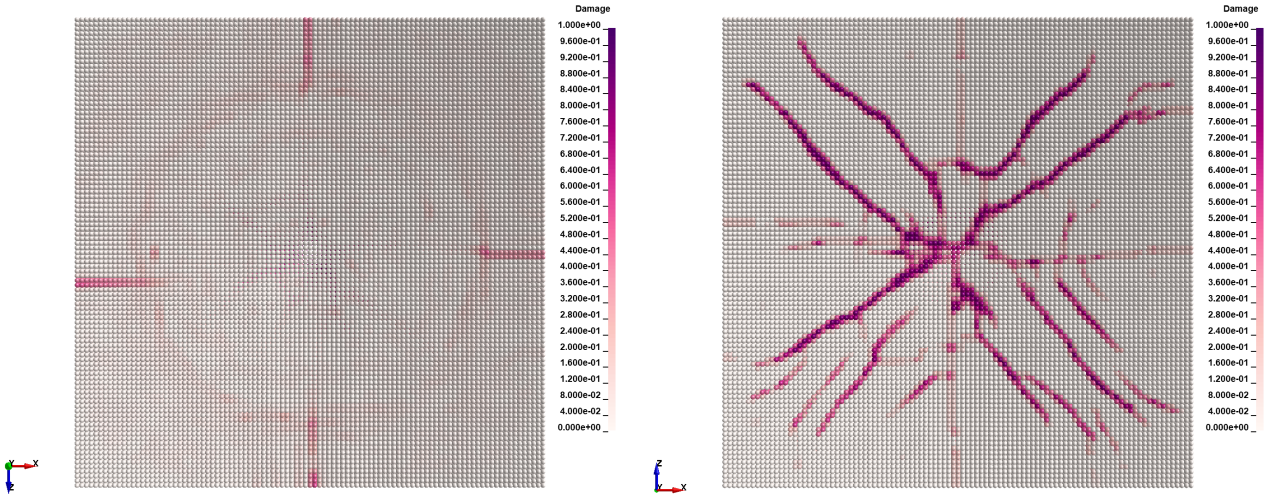

(a) top (b) bottom

Fig. 9.6. Damage of the model without the CSCM strain-rate effects.

Overall, as in the previous experiment, the SPH part of the model performed well, without any stability issues. The fact that the coupled SPH model was able to capture all the responses of the experiment is not only a proof that SPH is fully functional and can be used in civil engineering applications, but also that the proposed coupling approach works.

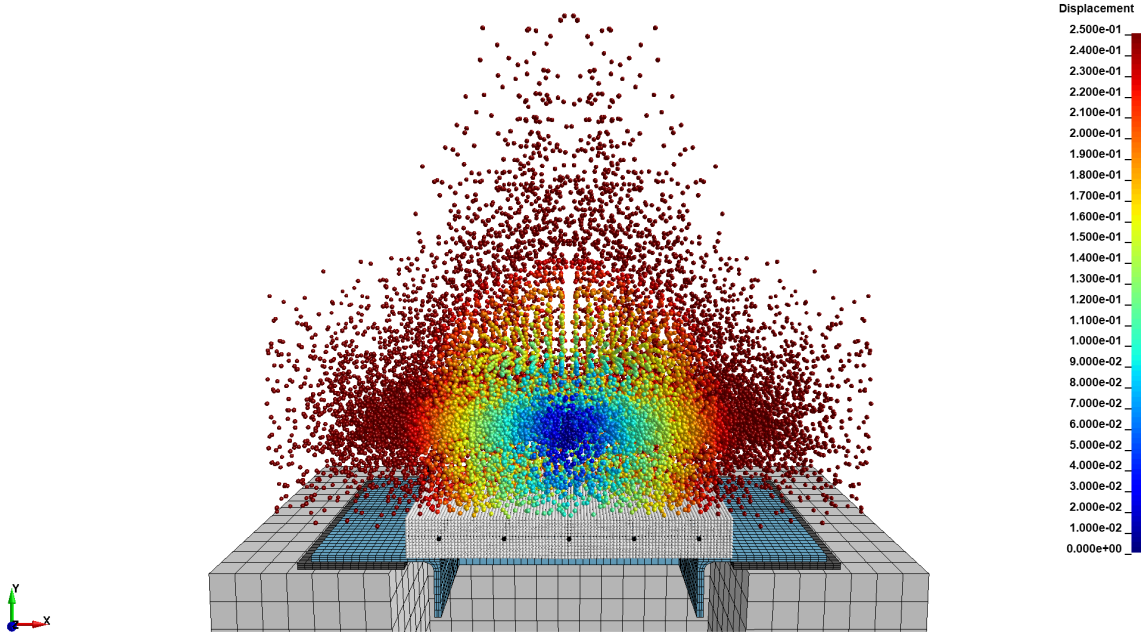

Fig. 9.7. Detonation of the TNT charge simulated with SPH (cross-section).

10 Conclusion

The main goal of the thesis was to provide a sufficient mathematical and application proof of the SPH utilization in fields of structural dynamics with an emphasis on quasi-brittle materials. The thesis offered not only one but many verifications and validations supported with experiments and benchmarks. That said, the main goal of the thesis was fulfilled.

In detail, the thesis provided a comprehensive overview of the SPH history, theory, mathematical implementation, modifications, and state-of-the-art corrections with respect to structural dynamics. The theoretical part was supplemented by a number of examples which show how to use the method, what to expect, where to be cautious, and what are the strengths and weaknesses of SPH. Since the author is aware of the considerable popularity of FEM, a chapter was dedicated to coupled SPH-FEM models. Three different coupling approaches were discussed in detail, subsequently compared and verified in a study. It was proved the methods are interchangeable.

Since it was found there is a significant gap in the research on quasi-brittle materials within the SPH framework, the author decided to improve that and provide as many answers as possible in the thesis. Demonstrations were carried out with the CSCM

material model, a representative of the quasi-brittle material models. To prove the functionality of SPH with CSCM, two well known experiments were simulated. It was proved that SPH is able to reproduce the behaviour observed in the experiments, it is not dependent on the discretization density, the normalization of the fracture energy is stable within the SPH framework, and that irregular subdomains of clustered SPH particles can be resolved with an adapted size of the support domain. Furthermore, the concept of the FEM erosion with transformation of the eroded mass into SPH was shown and validated on the experiment.

Since it is not likely that concrete would be used without any reinforcement, a chapter dedicated to the numerical modelling of reinforced concrete with SPH was also included. It is a well known fact that SPH suffers from a numerical instability, the so-called *tensile instability*, which makes it difficult to simulate a reinforcement. For that reason, the author proposed a new approach for the reinforcement modelling based on the *sublayer coupling* of SPH and FEM. The approach keeps the SPH adaptivity while taking advantage of FEM beam elements. The results presented in the chapter are therefore significant findings with a high potential for a real application.

Concrete structure is very complex which leads to a variability in experimental measurements although the tested specimens might be visually identical. In contrast, numerical simulations can and do return identical responses if there is no variability in input parameters. To get closer to reality, the author proposed the *algorithm for concrete structure generation*. The idea is based on utilization of spatial noise functions. This rather abstract technique proved to be robust, stable, and able to provide a generated spatial geometry of concrete which can be further used with SPH models. Combining the algorithm for concrete structure generation with material parameters oscillations, the so-called *numerical heterogeneity* can be implemented.

The last two chapters focused on the application of SPH in practice, validated with data from two experiments. The first experiment was a pure structural in which a reinforced concrete beam was subjected to an impact load. In essence, it is very difficult to simulate an HVI of a reinforced concrete with SPH. However, it was proved that with the proposed sublayer coupling approach for the reinforcement implementation such experiments can be simulated. Furthermore, the performance and stability of SPH with CSCM was validated. It was proved that using CSCM within the SPH framework offers a generic tool for civil engineering problems. The second experiment focused on a blast load in which the subject of the study was a reinforced concrete slab and the charge itself. Using the proposed sublayer coupling with FEM it was possible to match the experimental measurements. Furthermore, it was proved that SPH can perform coupled FSI simulations without any additional treatment.

With respect to the summary of the outcomes and findings written in this chapter, the thesis met the expected results and all the goals defined in section *Goals of the Thesis* were fulfilled.

References

[1] Lucy, L. B., "A Numerical Approach to the Testing of the Fission Hypothesis," *The Astronomical Journal*, vol. 82, no. 12, pp. 1013–1024, Dec. 1977. DOI: 10.1086/112164.

[2] Gingold, R. A. and Monaghan, J. J., "Smoothed Particle Hydrodynamics: Theory and Application to Non-Spherical Stars," *Monthly Notices of the Royal Astronomical Society*, vol. 181, no. 3, pp. 375–389, 1977. DOI: 10.1093/mnras/181.3.375.

[3] Fugelso, E. and Taylor, J. W., "Evaluation of Combined Obliquity and Yaw for U-0.75% Ti Penetrators," Los Alamos National Laboratory, Los Alamos, NM, United States, Technical Report LA-7402-MS, 1978.

[4] Morris, J. P., "Analysis of Smoothed Particle Hydrodynamics with Applications," Ph.D. dissertation, Monash University, 1996.

[5] Liu, G. R. and Liu, M. B., *Smoothed Particle Hydrodynamics: A Meshfree Particle Method*, First Edition. Singapore: World Scientific Publishing Co. Pte. Ltd., Oct. 2003, ISBN: 981-238-456-1. DOI: 10.1142/5340.

[6] Benz, W., "Smoothed Particle Hydrodynamics: A Review," in *The Numerical Modeling of Non-Linear Stellar Pulsation: Problems and Prospects*, J. R. Buchler, Ed., Boston: Kluwer Academic Publishers, 1990, pp. 269–288. DOI: 10.1007/978-94-009-0519-1_16.

[7] Randles, P. W. and Libersky, L. D., "Smoothed Particle Hydrodynamics: Some Recent Improvements and Applications," *Computer Methods in Applied Mechanics and Engineering*, vol. 139, no. 1–4, pp. 375–408, 1996. DOI: 10.1016/S0045-7825(96)01090-0.

[8] Liu, M. B. and Liu, G. R., *Particle Methods for Multi-Scale and Multi-Physics*, First Edition. Singapore: World Scientific Publishing Co. Pte. Ltd., Feb. 2016, ISBN: 978-981-4571-69-2. DOI: 10.1142/9017.

[9] Monaghan, J. J. and Lattanzio, J. C., "A Refined Particle Method for Astrophysical Problems," *Astronomy and Astrophysics*, vol. 149, no. 1, pp. 135–143, 1985. [Online]. Available: https://ui.adsabs.harvard.edu/abs/1985A&A...149..135M.

[10] Swegle, J. W., Hicks, D. L., and Attaway, S. W., "Smoothed Particle Hydrodynamics Stability Analysis," *Journal of Computational Physics*, vol. 116, no. 1, pp. 123–134, 1995. DOI: 10.1006/jcph.1995.1010.

[11] O'Brien, G. G., Hyman, M. A., and Kaplan, S., "A Study of the Numerical Solution of Partial Differential Equations," *Journal of Mathematics and Physics*, vol. 29, no. 1–4, pp. 223–251, 1950. DOI: 10.1002/sapm1950291223.

[12] Swegle, J. W., "SPH in Tension," Sandia National Laboratories, Albuquerque, NM, United States, Technical Report, 1992.

[13] Parshikov, A. N. and Medin, S. A., "Smoothed Particle Hydrodynamics Using Interparticle Contact Algorithms," *Journal of Computational Physics*, vol. 180, no. 1, pp. 358–382, 2002. DOI: 10.1006/jcph.2002.7099.

[14] Dyka, C. T. and Ingel, R. P., "An Approach for Tension Instability in Smoothed Particle Hydrodynamics (SPH)," *Computers & Structures*, vol. 57, no. 4, pp. 573–580, 1995. DOI: 10.1016/0045-7949(95)00059-P.

[15] Rubin, M. B., "Simple, Convenient Isotropic Failure Surface," *Journal of Engineering Mechanics*, vol. 117, no. 2, pp. 348–369, 1991. DOI: 10.1061/(ASCE)0733-9399(1991)117:2(348).

[16] Ožbolt, J., Bede, N., Sharma, A., and Mayer, U., "Dynamic Fracture of Concrete L-Specimen: Experimental and Numerical Study," *Engineering Fracture Mechanics*, vol. 148, pp. 27–41, 2015. DOI: 10.1016/j.engfracmech.2015.09.002.

[17] Buchar, J., Krejčí, J., and Forejt, M., "Response of Concrete to the Impact of Fragments Simulating Projectiles," *Engineering Mechanics*, vol. 8, no. 1, pp. 63–69, 2001, ISSN: 1805-4633.

[18] CEN, "EN 1992-1-1 Eurocode 2: Design of Concrete Structures – Part 1-1: General Ruels and Rules for Buildings," European Committee for Standardization, Brussels, Belgium, Standard EN 1992-1-1, Jul. 2018.

About the Author

Ing. Martin Hušek
Institute of Structural Mechanics
Faculty of Civil Engineering
Brno University of Technology
Veveří 331/95, 602 00 Brno
Czech Republic

Email: husek.m@fce.vutbr.cz

Education

2015 – present
Brno University of Technology, Faculty of Civil Engineering

- doctoral student

2013 – 2015
Brno University of Technology, Faculty of Civil Engineering

- master's degree in civil engineering
- thesis: London Eye

2009 – 2013
Brno University of Technology, Faculty of Civil Engineering

- bachelor's degree in civil engineering
- thesis: Design and Assessment of the Timber Dome

Professional Experience

2020 – present
Ansys, Inc.

- application engineering and consulting
- hydraulic fracturing simulator development
- 3D design

2018 – 2020
Dynardo GmbH

- application engineering and consulting
- high energy events simulations
- material calibration

2016 – 2020
Brno University of Technology

- project lead and research fellow
- preparation and realization of experiments
- university teaching

2014 – 2018
CENTURY 21 Doma

- interior, exterior, and product visualization
- graphic design

2012 – 2014
JK – STAVPROJEKT, s.r.o.

- civil engineering design
- building surveys

Research Projects

2017 – 2020
GA17-23578S
Damage Assessment Identification for Reinforced Concrete Subjected to Extreme Loading

- research fellow
- meshfree and coupled SPH-FEM simulations
- development of the algorithm for material structure generation

2017 – 2020
FV20372
The Software Tool for the Nonlinear Analysis of Concrete Structures During Fast Dynamic Processes

- research fellow
- material calibration

2017 – 2019
TH02020301
Advanced Design of Strengthening of Steel Structures Under Loading

- research fellow
- numerical models verifications

2017
FAST-J-17-4264
Experimental and Numerical Verifications of Meshfree Methods in Cases of Dynamically Loaded Concrete Structures

- project lead and research fellow
- meshfree and coupled SPH-FEM simulations

2016 – 2017
FAST-S-16-3718
Advanced Numerical Methods with Complex Material Models

- research fellow
- coupled SPH-FEM simulations and material calibration

2016
FAST-J-16-3684
Utilization of Particle Models in Simulations of Concrete Under Dynamic Load

- project lead and research fellow
- meshfree simulations

2015 – 2019
NPU LO1408
Advanced Building Materials, Constructions, and Technologies

- research fellow
- meshfree and coupled SPH-FEM simulations

2015 – 2016
GA14-25320S
Aspects of the Use of Complex Nonlinear Material Models

- research fellow
- high energy events simulations

Awards and Recognitions

2016

- 18th International Conference of Ph.D. Students JUNIORSTAV 2016: best paper of section 2.7 Structural Mechanics and best domestic paper of the conference

2015

- recognition for excellent study results during the master's study
- recognition for an exemplary diploma thesis and its defence during the final state examination
- medal Signum Prosperitatis for excellent academic results

2013

- recognition for excellent study results during the bachelor's study
- recognition for an exemplary bachelor's thesis and its defence during the final state examination

List of Publications

total publications = 36
h-index = 3

Journals with Impact Factor

[1] Nariman, N. A., Hušek, M., Mohammad, I. I., Ahmed, K. O., Dilshad, D., and Khidr, I., "Analysis of Stiffness and Flexural Strength of a Reinforced Concrete Beam Using an Invented Reinforcement System," *Frontiers of Structural and Civil Engineering*, pp. 1–12, 2021, IF: 1.680 (2019), JCR: Q3 (Engineering, Civil). DOI: 10.1007/s11709-021-0706-z.

[2] Hušek, M. and Kala, J., "Uncertainties in Blast Simulations Evaluated with Smoothed Particle Hydrodynamics Method," *Structural Engineering and Mechanics, An International Journal*, vol. 74, no. 6, pp. 771–787, 2020, IF: 3.101 (2019), JCR: Q1 (Engineering, Civil), JCR: Q2 (Engineering, Mechanical). DOI: 10.12989/sem.2020.74.6.771.

[3] Hušek, M. and Kala, J., "Material Structure Generation of Concrete and Its Further Usage in Numerical Simulations," *Structural Engineering and Mechanics, An International Journal*, vol. 68, no. 3, pp. 335–344, 2018, IF: 3.017 (2018), JCR: Q1 (Engineering, Civil), JCR: Q2 (Engineering, Mechanical). DOI: 10.12989/sem.2018.68.3.335.

[4] Kala, J. and Hušek, M., "Improved Element Erosion Function for Concrete-Like Materials with the SPH Method," *Shock and Vibration*, vol. 2016, pp. 1–13, 2016, IF: 1.158 (2016), JCR: Q3 (Mechanics), JCR: Q3 (Acoustics), JCR: Q4 (Engineering, Mechanical). DOI: 10.1155/2016/4593749.

Journals in Scopus Database

[5] Hušek, M., Král, P., Kala, J., Hradil, P., and Maňas, P., "Concrete Targets with Heterogeneities under Impact Loading," *Advances in Military Technology*, vol. 13, no. 1, pp. 107–118, 2018. DOI: 10.3849/aimt.01216.

[6] Král, P., Hušek, M., Hradil, P., Kala, J., and Maňas, P., "Identification of Concrete Material Model Parameters Using Optimisation Algorithms," *Advances in Military Technology*, vol. 13, no. 1, pp. 33–45, 2018. DOI: 10.3849/aimt.01213.

[7] Hušek, M. and Kala, J., "How to Get Closer to Reality in Pressure Test Simulations with the SPH Method," *International Journal of Mechanics*, vol. 11, pp. 226–233, 2017. [Online]. Available: http://www.naun.org/main/NAUN/mechanics/2017/a642003-aan.pdf.

[8] Hokeš, F., Hušek, M., Kala, J., and Král, P., "Predicting the Load-Carrying Capacity of Reinforced Concrete Structural Element," *WSEAS Transactions on Applied and Theoretical Mechanics*, vol. 12, pp. 1–10, 2017. [Online]. Available: http://www.wseas.org/multimedia/journals/mechanics/2017/a025811-081.pdf.

[9] Hušek, M., Kala, J., Král, P., and Hokeš, F., "Effect of the Support Domain Size in SPH Fracture Simulations," *International Journal of Mechanics*, vol. 10, pp. 396–402, 2016. [Online]. Available: http://www.naun.org/main/NAUN/mechanics/2016/b162003-208.pdf.

[10] Kala, J. and Hušek, M., "High Speed Loading of Concrete Constructions with Transformation of Eroded Mass into the SPH," *International Journal of Mechanics*, vol. 10, pp. 145–150, 2016. [Online]. Available: http://www.naun.org/main/NAUN/mechanics/2016/a442003-194.pdf.

[11] Hokeš, F., Hušek, M., Král, P., and Kala, J., "Numerical Simulation of Reinforced Concrete Beam with Utilization of Elasto-Plastic Material Model of Concrete," *WSEAS Transactions on Applied and Theoretical Mechanics*, vol. 11, pp. 136–141, 2016. [Online]. Available: http://www.wseas.org/multimedia/journals/mechanics/2016/a325811-092.pdf.

Peer-Reviewed Journals

[12] Hušek, M., Hokeš, F., Kala, J., and Král, P., "Inclusion of Randomness into SPH Simulations," *WSEAS Transactions on Heat and Mass Transfer*, vol. 12, pp. 1–10, 2017. [Online]. Available: http://www.wseas.org/multimedia/journals/heat/2017/a025812-166.pdf.

[13] Hušek, M., Hokeš, F., Kala, J., and Král, P., "A Simple Solution for Randomized Failure Modeling with the SPH Method," *International Journal of Theoretical and Applied Mechanics*, vol. 1, pp. 253–258, 2016. [Online]. Available: http://www.iaras.org/iaras/filedownloads/ijtam/2016/009-0038.pdf.

[14] Hušek, M., Kala, J., Hokeš, F., and Král, P., "How to Handle Irregular Distribution of SPH Particles in Dynamic Fracture Analysis," *International Journal of Theoretical and Applied Mechanics*, vol. 1, pp. 212–217, 2016. [Online]. Available: http://www.iaras.org/iaras/filedownloads/ijtam/2016/009-0032.pdf.

Conference Papers

[15] Hušek, M., Kala, J., Král, P., and Hokeš, F., "Using Noise to Generate the Material Structure of Concrete," in *Proceedings of the 15th International Conference of Numerical Analysis and Applied Mathematics*, ser. AIP Conference Proceedings, ICNAAM, vol. 1978, Thessaloniki, Greece, Sep. 2018, pp. 1–4. DOI: 10.1063/1.5044017.

[16] Němec, I., Vaněčková, A., and Hušek, M., "Nonlinear Seismic Analysis by Explicit and Implicit Method," in *Proceedings of the 15th International Conference of Numerical Analysis and Applied Mathematics*, ser. AIP Conference Proceedings, ICNAAM, vol. 1978, Thessaloniki, Greece, Sep. 2018, pp. 1–4. DOI: 10.1063/1.5044022.

[17] Král, P., Hradil, P., Hušek, M., Kala, J., and Kala, Z., "Sensitivity Analysis and Optimization as Tools for the Inverse Concrete Material Model Parameter Identification," in *Proceedings of the 15th International Conference of Numerical Analysis and Applied Mathematics*, ser. AIP Conference Proceedings, ICNAAM, vol. 1978, Thessaloniki, Greece, Sep. 2018, pp. 1–4. DOI: 10.1063/1.5044025.

[18] Hušek, M., "Effect of Wind Wave on Structures," in *Proceedings of the 20th International Conference of Ph.D. Students JUNIORSTAV 2018*, FAST VUT, Brno, Czech Republic, Jan. 2018, pp. 1–6.

[19] Hušek, M., Kala, J., Král, P., and Hokeš, F., "Concept and Numerical Simulations of a Reactive Anti-Fragment Armour Layer," in *Proceedings of the 14th International Conference of Numerical Analysis and Applied Mathematics*, ser. AIP Conference Proceedings, ICNAAM, vol. 1863, Rhodes, Greece, Sep. 2017, pp. 1–4. DOI: 10.1063/1.4992643.

[20] Král, P., Hradil, P., Hušek, M., and Hokeš, F., "Comparison of Responses of Concrete Damage Material Models with Respect to Optimization-Based Material Parameter Identification," in *Proceedings of the 14th International Conference of Numerical Analysis and Applied Mathematics*, ser. AIP Conference Proceedings, ICNAAM, vol. 1863, Rhodes, Greece, Sep. 2017, pp. 1–4. DOI: 10.1063/1.4992644.

[21] Hušek, M., Kala, J., Hokeš, F., and Král, P., "Conversion of Fractal Fields into Heterogeneities inside SPH Simulations," in *Proceedings of the World Multidisciplinary Civil Engineering-Architecture-Urban Planning Symposium 2017*, ser. IOP Conference Series: Materials Science and Engineering, WMCAUS, vol. 245, Prague, Czech Republic, Jan. 2017, pp. 1–7. DOI: 10.1088/1757-899X/245/3/032024.

[22] Hušek, M., Kala, J., Král, P., and Hokeš, F., "Steel Fibre Reinforced Concrete Simulation with the SPH Method," in *Proceedings of the World Multidisciplinary Civil Engineering-Architecture-Urban Planning Symposium 2017*, ser. IOP Conference Series: Materials Science and Engineering, WMCAUS, vol. 245, Prague, Czech Republic, Jan. 2017, pp. 1–8. DOI: 10.1088/1757-899X/245/3/032070.

[23] Hokeš, F., Král, P., Hušek, M., and Kala, J., "Study on Identification of Material Model Parameters from Compact Tension Test on Concrete Specimens," in *Proceedings of the World Multidisciplinary Civil Engineering-Architecture-Urban Planning Symposium 2017*, ser. IOP Conference Series: Materials Science and Engineering, WMCAUS, vol. 245, Prague, Czech Republic, Jan. 2017, pp. 1–10. DOI: 10.1088/1757-899X/245/3/032079.

[24] Král, P., Hokeš, F., Hušek, M., Kala, J., and Hradil, P., "Optimization-Based Inverse Identification of the Parameters of a Concrete Cap Material Model," in *Proceedings of the World Multidisciplinary Civil Engineering-Architecture-Urban Planning Symposium 2017*, ser. IOP Conference Series: Materials Science and Engineering, WMCAUS, vol. 245, Prague, Czech Republic, Jan. 2017, pp. 1–10. DOI: 10.1088/1757-899X/245/3/032078.

[25] Hušek, M., Král, P., Kala, J., Hradil, P., and Maňas, P., "Simulating Randomized Failure of Concrete Targets," in *Proceedings of the 6th International Conference on Military Technologies*, ICMT, Brno, Czech Republic, May 2017, pp. 303–307. DOI: 10.1109/MILTECHS.2017.7988774.

[26] Král, P., Hušek, M., Hradil, P., Kala, J., and Maňas, P., "Optimization of the Material Parameters of the Continuous Surface Cap Model for Concrete," in *Proceedings of the 6th International Conference on Military Technologies*, ICMT, Brno, Czech Republic, May 2017, pp. 298–302. DOI: 10.1109/MILTECHS.2017.7988773.

[27] Hokeš, F., Král, P., Krňávek, O., and Hušek, M., "Improved Sensitivity Analysis in the Inverse Identification of the Parameters of a Nonlinear Material Model," in *Proceedings of the 12th International Conference of Modern Building Materials, Structures and Techniques*, ser. Procedia Engineering, MBMST, vol. 172, Vilnius, Luthuania, May 2017, pp. 347–354. DOI: 10.1016/j.proeng.2017.02.039.

[28] Král, P., Hradil, P., Kala, J., Hokeš, F., and Hušek, M., "Identification of the Parameters of a Concrete Damage Material Model," in *Proceedings of the 12th International Conference of Modern Building Materials, Structures and Techniques*, ser. Procedia Engineering, MBMST, vol. 172, Vilnius, Luthuania, May 2017, pp. 578–585. DOI: 10.1016/j.proeng.2017.02.068.

[29] Hušek, M., "Tensile Instability Elimination with Smoothed Particle Galerkin Method," in *Proceedings of the 19th International Conference of Ph.D. Students JUNIORSTAV 2017*, FAST VUT, Brno, Czech Republic, Jan. 2017, pp. 1–8.

[30] Hokeš, F., Hušek, M., and Král, P., "Nonlinear Numerical Study of Pin Joint at Static and Cyclic Loading," in *Proceedings of the 19th International Conference of Ph.D. Students JUNIORSTAV 2017*, FAST VUT, Brno, Czech Republic, Jan. 2017, pp. 1–7.

[31] Král, P. and Hušek, M., "Concrete in Uniaxial and Triaxial Compression – Experimental and Numerical Analysis in Interaction with Material Parameter Optimization," in *Proceedings of the 19th International Conference of Ph.D. Students JUNIORSTAV 2017*, FAST VUT, Brno, Czech Republic, Jan. 2017, pp. 1–9.

[32] Hušek, M., Kala, J., Hokeš, F., and Král, P., "Influence of SPH Regularity and Parameters in Dynamic Fracture Phenomena," in *Proceedings of the World Multidisciplinary Civil Engineering-Architecture-Urban Planning Symposium 2016*, ser. Procedia Engineering, WMCAUS, vol. 161, Prague, Czech Republic, Jan. 2016, pp. 489–496. DOI: 10.1016/j.proeng.2016.08.671.

[33] Hokeš, F., Kala, J., Hušek, M., and Král, P., "Parameter Identification for a Multivariable Nonlinear Constitutive Model inside ANSYS Workbench," in *Proceedings of the World Multidisciplinary Civil Engineering-Architecture-Urban Planning Symposium 2016*, ser. Procedia Engineering, WMCAUS, vol. 161, Prague, Czech Republic, Jan. 2016, pp. 892–897. DOI: 10.1016/j.proeng.2016.08.743.

[34] Hušek, M., "A Brief Look into the Terminal Ballistics," in *Proceedings of the 18th International Conference of Ph.D. Students JUNIORSTAV 2016*, FAST VUT, Brno, Czech Republic, Jan. 2016, pp. 1–7.

[35] Kala, J. and Hušek, M., "Useful Material Models of Concrete when High Speed Penetrating Fragments are Involved," in *Proceedings of the 9th International Conference on Continuum Mechanics*, WSEAS, Rome, Italy, Nov. 2015, pp. 190–193. [Online]. Available: http://www.wseas.us/e-library/conferences/2015/Rome/NRG/NRG-28.pdf.

[36] Hušek, M., "Validation of Empirical Equations for Penetration Prediction of Concrete Specimens with Numerical Simulations," in *Proceedings of the 23rd SVSFEM ANSYS Users' Group Meeting and Conference 2015*, SVS FEM s.r.o., Hustopeče, Czech Republic, Jun. 2015, pp. 44–63. [Online]. Available: https://aum.svsfem.cz/files/AUM2015.pdf.

Abstract

The focus of the thesis is on the application of the Smoothed Particle Hydrodynamics (SPH) method in structural dynamics with an emphasis on usage of quasi-brittle materials. The thesis is divided into several parts to provide a comfortable transition between the theory and application. The first part is focused on the introduction, history, and theoretical background of SPH. Numerical examples in which strengths and weaknesses of SPH are shown follow. In addition to pure SPH models, several coupling approaches with the Finite Element Method (FEM) are also discussed.

After the introduction of SPH, the focus is on quasi-brittle materials and their reinforced variants. The numerical concept and mathematical background of the Continuous Surface Cap Model (CSCM) are outlined, several benchmarks are presented. Strain-rate effects and their impact on pure SPH and coupled SPH-FEM models are evaluated next. In this section, the author proposes a new approach for SPH models reinforcement with FEM beam elements while strengths of both methods are preserved. The coupling approach was named *sublayer coupling* and shows a potential in simulations while the SPH tensile instability is alleviated.

Since concrete is often associated with heterogeneity and very specific material structure, a unique *algorithm for concrete structure generation* in combination with SPH is proposed in the next chapter. The concept is based on utilization of coherent noise functions which can bring a variability to numerical models. It has been proved that the algorithm is robust, stable, and easy to implement into the SPH framework. With regard to that, the so-called *numerical heterogeneity*, a concept of parameters variability implementation, is introduced together with examples.

The last part of the thesis is dedicated to the application of SPH in real experiments, specially designed to test SPH to the full. The first experiment focuses on a high velocity impact (HVI) in which the functionality of the proposed approach of the sublayer reinforcement coupling is demonstrated. The second experiment deals with an explosion (blast load) in which the focus is on both the loaded specimen and charge. Since SPH simulates the explosive, detonation products, and the loaded specimen, it is in fact a fully coupled fluid-structure interaction (FSI) simulation. Furthermore, the SPH reinforcement with the sublayer coupling is tested again, yet for much higher load rate. The constitutive model strain-rate effects are also the subject of the study in both experiments.

Conclusions are discussed at the end of the thesis.

Abstrakt

Disertační práce je zaměřena na aplikaci metody Smoothed Particle Hydrodynamics (SPH) ve strukturální dynamice s důrazem na použití kvazi-křehkých materiálů. Disertační práce je rozdělena do několika částí tak, aby došlo k plynulému navázání mezi teorií a aplikací. První část je zaměřena na úvod, historii a teoretické pozadí SPH. Numerické příklady, kde jsou ukázány silné a slabé stránky SPH, následují. Diskutovány jsou rovněž metody tvorby kombinovaných modelů s Finite Element Method (FEM).

Po úvodu do SPH se práce soustředí na kvazi-křehké materiály a jejich vyztužené varianty. Nastíněny jsou numerické koncepty a matematické pozadí Continuous Surface Cap Model (CSCM) spolu s několika benchmarky. Následuje rozbor vlivu rychlosti přetvoření na modely SPH a na kombinované modely SPH-FEM. V této sekci autor představuje nový způsob vyztužení modelů SPH s pomocí nosníkových prvků FEM, zatímco jsou silné stránky obou metod zachovány. Tento způsob spojení byl nazván *vazba podvrstvou* a ukazuje potenciál v simulacích, zatímco je tahová nestabilita SPH zmírněna.

Jelikož je beton často spojován s heterogenitou a velmi specifickou materiálovou strukturou, unikátní *algoritmus pro generaci struktury betonu* v kombinaci s SPH je představen v následující kapitole. Koncept je založen na využití koherentních funkcí šumu, které mohou přinést variabilitu do numerických modelů. Bylo prokázáno, že algoritmus je robustní, stabilní a jednoduchý na implementaci do SPH. S ohledem na to, takzvaná *numerická heterogenita*, koncept implementace parametrové variability, je představena spolu s příklady.

Poslední část práce je zaměřena na aplikaci SPH ve skutečných experimentech, speciálně navržených pro otestování SPH jak jen to lze. První experiment se soustředí na náraz ve vysoké rychlosti (HVI), kde je prokázána funkcionalita navrhovaného způsobu vyztužení s podvrstvou. Druhý experiment se zabývá výbuchem (zatížení tlakovou vlnou), kde zaměření je na zatěžovaný vzorek a nálož. Vzhledem k tomu, že SPH simuluje nálož, plyny výbuchu a zatěžovaný vzorek, jedná se ve skutečnosti o plně svázanou simulaci interakce tekutiny a struktury (FSI). Navrhovaný způsob vyztužení s podvrstvou je znovu testován, avšak pro mnohem vyšší rychlosti zatížení. Efekty vlivu rychlosti přetvoření implementovaného do konstitučního modelu jsou rovněž předmětem zkoumání v obou experimentech.

Závěry jsou diskutovány na konci práce.